Joaquina Zappey


# [RADIONUCLIDE MIGRATION IN THE NEAR FIELD OF A GEOLOGICAL REPOSITORY]

The influence of competition on the molecular diffusion coefficient of pertechnetate and selenite in bentonite.

**The influence of competition on the molecular diffusion coefficient of pertechnetate and selenate in bentonite.**

Joaquina Zappey
1319981

**Master thesis performed at:**

Section Radiation and Isotopes for Health
Radiation, Radionuclides & Reactors
Faculty of Applied Science
Delft University of Technology

**Under supervision of:**

Prof. Dr. R.J.M Konings

**Graduation Committee:**

Prof. dr. R.J.M Konings
Prof. dr. H.T. Wolterbeek
Dr.ir. A.G. Denkova

**7 October 2013**

*Little did I know was that my master thesis would be the most fun I would have during my university education. Conducting your own research and writing a report about it may indeed sometimes be challenging, but the freedom to do your own thing and the section I got into make it up.*

*Of course, I did not brought this thesis to a successful ending by myself so I would like to thank the following people:*

*Rudy Konings, my prof. and supervisor. Thank you for supervision.*

*All the students of RIH for making it a fun year and helping: Robin Arentien Alex and Anca.*

*Dennis Bykov, for revising my report.*

*The SBD for opening the bar every Friday ;)*
*Henk and Koos*

*My graduation committee:*
*Antonia Denkova and Bert Wolterbeek.*

Deep geological storage is one of the solutions proposed for the long-term storage of nuclear waste. Various countries have already been exploring the option of storing nuclear waste underground at a depth of 300 to 800 meters. Such a deep geological storage facility would consist of several engineered barriers and a natural barrier, the natural host formation. In the Netherlands and Belgium, natural occurring Boom Clay has been identified as a potential host formation.

Boom clay is a smectite rich clay and a complementary buffer material would be Bentonite. Bentonite is also a smectite rich clay and under conditions found in the Netherlands and Belgium, they both have a low hydraulic gradient, a reducing environment and a slightly alkaline pH. These and other characteristics make it that the migration of radionuclides is diffusion controlled. This is a desirable characteristic.

During this thesis, we set out to build and test an electromigration cell and research the competition of radionuclides in the near field. The elements researched are ceasium, technetium and selenium. Ceasium was chosen as it is a widely research elements and much data on it can be found. This data was used to compare our data and with that to revise the migration cell.

The apparent molecular diffusion coefficient ($D_{app}$) of Ceasium found was $9 \cdot 10^{-11}$ [$m^2/s$] at a dry density of $0.9 \cdot 10^3$ [$kg/m^3$], which is in agreement with results found in literature $1.4 \cdot 10^{-11}$ [18]. The difference in radix could be due to be larger slice sizes used in this experiment, 4 mm instead of 1 mm, but also due to Bentonite being an organic material. There is no such thing as standardized Bentonite. The CEC, smectite content, porosity may change from Bentonite to Bentonite and even from sample to sample. The radices found in literature are therefore also diverging.

The experiment with Ceasium were done at both high (>25 mA) and low (<25 mA) current. Although the results can be mixed, a $R^2$ of ~0.88 was achieved, some suspicion exist that the current might influence the extent of dispersion. The dispersion at high current may be greater due to greater varieties in water velocity. Altogether, the results show that the electromigration cell works properly.

The second set of experiments was conducted with Technetium. Here we set out even more to shorten the experimental time and only high current experiments were done. The migration profiles show a typical Gaussian distribution profile, with a peak located sufficiently far away from the origin, after only three hours at a current of 40 mA. All other experiments also showed a typical Gaussian distribution profiles located away from the origin. Therefore, it is possible to reduce experimental time even further to less than 12 hours.

The $D_{app}$ obtained for Technetium was $2 \cdot 10^{-11}$ [$m^2/s$], which is normal and according to literature. A second matter we wanted to investigate is the retardation of Technetium. Technetium forms oxyanions and is deemed unretarded in it pertechnetate form. However, a small retardation of ~3.2-3.4 was found for technetium. The retardation is can be due to the complexion with the hydroxide ion of the Al-octahedrals.

During the mixed experiments (Tc and Se), the diffusion profiles of Tc showed four different peaks. Implying that the Technetium is immobilized and then once again remobilized. Hydrogen peroxide was used during this experiments. Therefore, a first suspicion is that the hydroxyls present in the clay sample immobilizes Tc and that later on the Tc is remobilized by the hydrogen peroxide.

| Symbol | Term | Unit | constant |
|---|---|---|---|
| | | | |
| $\alpha$ | Longitudinal dispersion | [m] | |
| $\varepsilon$ | Total porosity | [-] | |
| $\eta_{diff}$ | Diffusion accessible porosity | [-] | |
| $\mu$ | the viscosity of the fluid | [Pa·s] | |
| $\mu_e$ | ionic mobility, | [$m^2$/sV] | |
| $v_{eo}$ | electro-osmotic velocity | $[m/s]$ | |
| $\mu_{eo}$ | electro-osmotic mobility | $[m^2/Vs]$ | |
| $\rho_d$ | Dry grain density | [kg/$m^3$] | Also called bulk density |
| $\rho_l$ | Liquid density | [kg/$m^3$] | |
| $\rho_s$ | Grain density | [kg/$m^3$] | Also called particle density or true density |
| $\rho_w$ | Water density | [kg/$m^3$] | |
| $\tau$ | Tortousity | [-] | |
| D | Dispersion coefficient | [$m^2$/s] | |
| $D_i$ | Apparent dispersion coefficient | [$m^2$/s] | |
| $D_m$ | Molecular diffusion coefficient | [$m^2$/s] | |
| $D_{app}$ | Apparent molecular diffusion coefficient | [$m^2$/s] | |
| E | electrical field | [V/m] | |
| $e$ | electron charge | [C]. | $1.16 \cdot 10^{-19}$ |
| $K_b$ | the Boltzmann constant | [J/K] | $1.38 \cdot 10^{23}$ |
| $K_d$ | distribution coefficient | [$m^3$/kg] | |
| $R$ | radius of the particle | [m] | |
| R | Retardation factor | [-] | |
| $T$ | temperature | [K] | |
| q | charge of the particle | [-] | |
| $v$ | speed of the particle | [m/s] | |
| $V_{app}$ | Apparent convective velocity | [m/s] | |
| $V_c$ | Convective velocity | [m/s] | |
| $V_c^t$ | Total convective velocity | [m/s] | |
| $Z$ | valence | [−] | |
| | | | |

# 1. Introduction

Eliminating the risk of radionuclides leaching from radioactive waste stored underground to the biosphere is the goal set by all countries that make use of nuclear power and other nuclear applications. Several countries plan on geological disposal of radioactive waste in rocks, salt and clay sediments. The design principle is that highly radioactive waste, such as spent fuel and products from processed waste, is vitrified, enclosed in containers—canisters— and isolated by smectite or smectite-rich clay, at a depth between 300 and 800 meter.

Deep underground, the radioactive waste has to stay isolated until it has decayed to natural levels [5]. To fulfil this requirement of long-term isolation, a system of five complementary barriers has been designed. The barrier concept prevents deep ground waters, present in almost all rock formations, from rapidly leaching the waste and from transporting radioactivity away from the repository. The barriers can be classified as either engineered barriers, which are constructed in the repository, or natural barriers, which are in the surrounding geological environment. Figure 1 gives a schematic overview of the barriers between the radioactive waste and the biosphere.

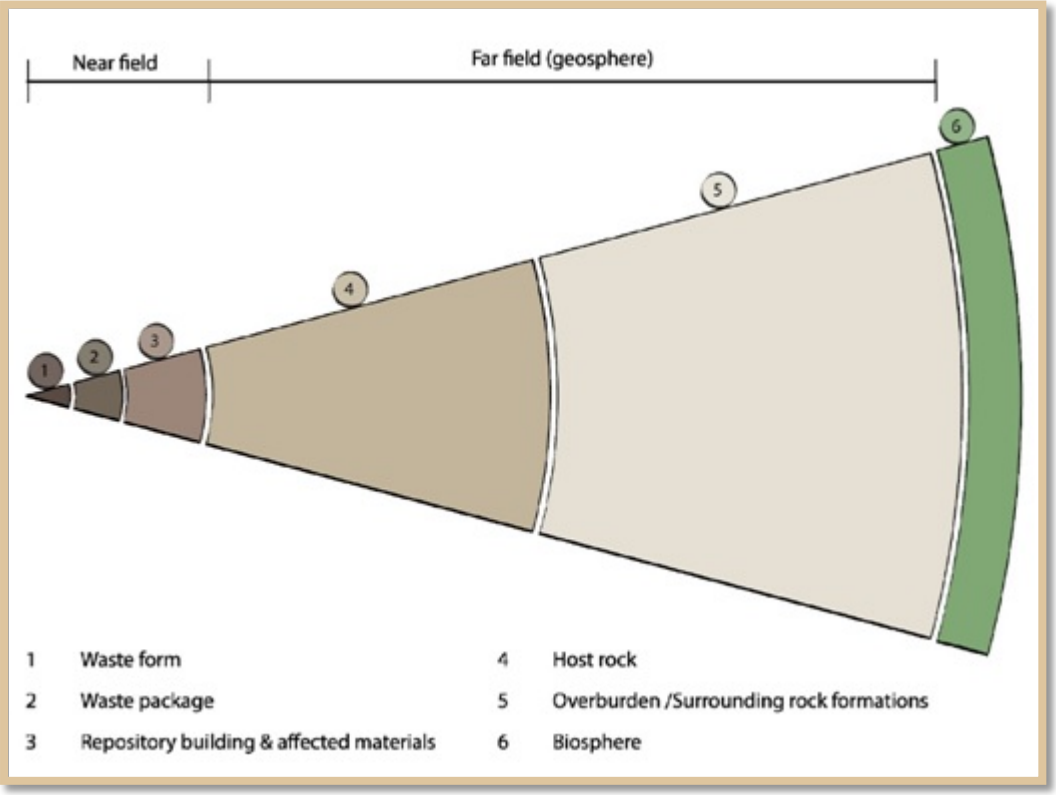


Figure 1: Schematic overview of the different barriers composing the deep geological storage [5].

For disposal in hard rocks and clays, the basic engineered barriers are: immobilization of the waste by vitrification, encapsulation of the solidified waste form in canisters, and surrounding of the canisters by a buffer or backfill material that fills the space between the container and the rock. The natural barriers are provided by the rocks and the overburden between the repository and Earth's surface (biosphere).

The canisters prevent water from reaching the waste. Its protective nature lasts for several hundreds to thousands of years, allowing enough time for most activity to decay in the waste matrix. The buffer surrounding the canister protects the canister from any mechanical disturbance and -prevents water from reaching the canister. It is also this buffer (backfill) material that will eventually contain the radionuclides after the canisters start to breach[6].

Together, these three barriers together make up the near field, see Figure 1. As a buffer material, bentonite is often used. Bentonite has excellent characteristics as a radionuclide barrier. It has a low hydraulic conductivity, a reducing potential, a slightly alkaline pH, a high cation exchange capacity (CEC) and a high plasticity. It is due to these properties that radionuclide migration through bentonite is extremely slow [7] which is exactly its purpose.

Much research has been done on radionuclide migration into the near field. Thus far, the focus always was on a single radionuclide and its geochemical behaviour. In this report, we will determine how the competition between different elements influences the migration.

In order to conduct these experiments within a reasonable time scale, an electromigration cell was built to speed up the process. Normally, migration experiments are done by pure diffusion tests or tests that have an additional hydraulic pressure. Such conventional experiments can take any time from months to a few years. With an electromigration cell, the experimental time can be reduced to a few hours or days. In this report, results will be extracted in just a few hours and compared to known data to determine if the results obtained are accurate.

Thus, the questions to be answered are:

(1) Did we build a functional electromigration cell?
(2) Can experimental time be reduced to hours?
(3) Does competition exist between technetium and selenium?

In Chapter 2 through 5, the theory will be explained. Starting with an overview of the different experimental set-up possible in Chapter 2. Following in Chapter 3, the mathematical background concerning the experiments will be given. And lastly, in Chapter 4 and 5, the retention processes present in clay will be handle and the geochemical behaviour of the research elements. In Chapter 6 and 7, the experimental methods and material will be described and the results obtained will be discussed. In the final Chapter 8, the conclusion and given en recommendations.

# 2. Overview of migration experiments

In this chapter, we briefly discuss the conventional experimental set-ups used. The conventional migration experiments are: percolation experiments, pulse injection experiments, through-diffusion experiments, and in-diffusion experiments.

Between these experiments, we can distinguish two experimental principles: the pure diffusion test, these experiments solely have a concentration gradient, and dispersion/advection experiments, these experiments have hydraulic pressure gradient next to their concentration gradient. The through-diffusion and in-diffusion experiments are pure diffusion experiments. The percolation and pulse injection experiments are dispersion/advection experiments.

Compared to electromigration, they all have one major disadvantage: the experimental time of these set-ups is much longer than the experimental time of an electromigration set-up. However, the conventional set-ups also have advantages over the electromigration set-up. The only parameter that can be derived with the electromigration experiments is the apparent molecular diffusion (Chapter 3), whereas the conventional techniques also allow deriving the porosity and the retardation factor experimentally [8].

## 2.1 Pure diffusion experiments

The pure diffusion test, i.e. without advection, has two different set-ups: the “through-diffusion” and “in-diffusion” experiments.

In a through-diffusion test, two well-stirred water compartments occlude the clay core on both sides. The tracer is added to the inlet compartment and diffuses through the clay core towards the outlet compartment. The tracer is measured at both the inlet and the outlet as a function of time. The inlet and outlet compartment are chosen such, that changes in concentration at the outlet compartment are negligible.

The in-diffusion experiment is similar to the through-diffusion experiment, with the difference that it has no outlet compartment. Thus, when the tracer does not reached the outlet compartment, a through-diffusion experiment becomes an in-diffusion test[9, 10].

## 2.2 Dispersion/advection experiments

The easiest set-up in the dispersion/advective test is the percolation set-up. The percolation test has an aliquot of tracer spiked either directly on the clay surface or on a filter paper. The tracer is sandwiched between two clay cores and these clay cores are once again sandwiched between two filters in a permeation cell. The cell is continuously percolated with liquid.

The set-up of the pulse injection experiment is similar to that of the percolation test, but rather than having two clay cores, the permeation cell has one clay core, which is sandwiched between two filters, and rather than having the tracer spiked in between de clay core, the tracer is spiked at the inlet. In both experiments, the water flowing out of the system is collected and the tracer concentration in the water is measured as a function of time [4,5].

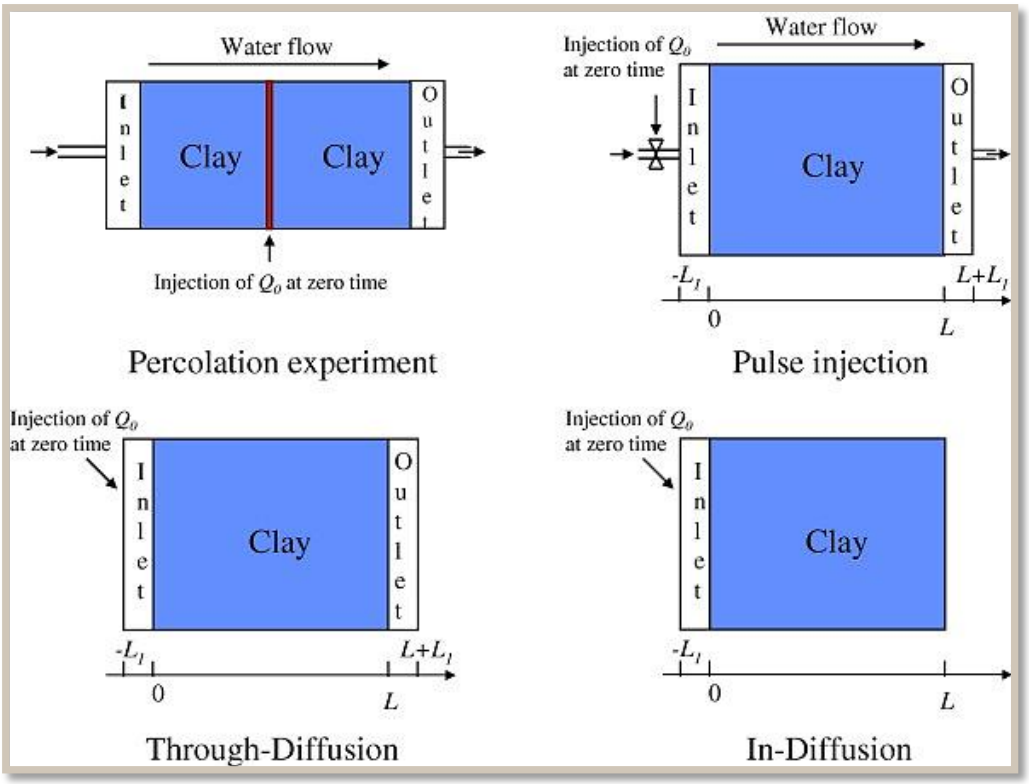


**Figure 2: a) Percolation Experiment. The tracer is spiked in between the two clay cores. The clay cores are confined by two water compartments. A hydraulic pressures in applied. b) Pulse injection: The tracer is spiked at the inlet. The clay core is confined between to water compartments. A hydraulic pressure is applied. c) Through diffusion: The tracer is spiked at the inlet. Tracer is measured at the inlet and outlet. No additional hydraulic pressure applied. d) In-diffusion: Tracer is spiked at the inlet. The tracer is measured at the inlet. No additional hydraulic pressure applied [4].**

## 2.3 Electromigration

By accelerating the migration of the radionuclides, the experimental time is reduced and more data can be retrieved within the same time frame, which increases the reliability of the measured parameters, by lowering the statistical error. Applying a hydraulic pressure can accelerate the migration, but bentonite has a very low hydraulic conductivity, so a very high hydraulic pressure must be applied to obtain the desired effect.

A more sophisticated way to enhance the migration is to apply an electric field over the sample. Small electrical fields can easily induce balanced flows that are otherwise only caused by large hydraulic pressure gradients. In this case, electrical fields are far more efficient to accelerate migration[11].

The electromigration cell exists of a sample holder confined between two water compartments. The current that is applied during the experiments cause the water in the water compartments to decompose into $O_2$ and $H_2$ (electrolysis). Through an oxidation reaction at the anode water is split to produces electrons. The electrons produced are then consumed during a reduction reaction at the anode. The reaction schemes are given in equation: 1.1, 1.2 and 1.3.

The reaction at both electrodes is:

$$2\ H_2O \leftrightarrow 2H^+\ (aq) + 2\ OH^-\ (aq) \qquad (1.1)$$

The reduction reaction at the cathode (eq. 1.2) and the oxidation reaction at the anode (eq. 1.3) are:

$$2H^+\ (aq) + 2e^- \rightarrow H_2\ (g) \qquad (1.2)$$

$$2\ OH\text{-}\ (aq) \rightarrow H_2O\ (l) + ½\ O_2\ (g) + 2e^- \qquad (1.3)$$

The overall reaction is:

$$H_2O\ (l) \xrightarrow{\text{electricity}} H_2\ (g) + ½\ O_2\ (g) \qquad (1.4)$$

Because the $OH^-$ produced at the cathode is not consumed, it remains in the water compartment forming an alkaline front that increases the pH at the cathode. The opposite event occurs at the anode, at the anode the $H^+$ produced is not consumed this leads to an acid front that decreases the pH. To counteract this effect two circuits are made each for every water compartment, which recycle the water back to an external reservoir where the hydrogen and hydroxide can recombine again, see Chapter 6 for a more detailed description of the cell.

# 3. Governing the transport equation for electrokinetic transport through a porous medium

The goal of building an electromigration cell is to speed up the process of obtaining apparent molecular diffusion coefficients in clay. In this chapter, we derive the transport equation for electrokinetic transport through a porous medium. With this transport equation, one is able to calculate the diffusion coefficient, the parameter of interest. In Section 3.1, the equations and physics concerning electromigration and electro-osmosis are explained. This is followed by a general overview of mass transport of chemical species in section 3.2. In the last paragraph, we set out to derive the molecular diffusion coefficient and to give an analytical solution to the ordinary differential equation, which is used to fit the experimental data.

## 3.1 Electromigration and electro-osmosis

When a potential gradient is applied over a water-saturated porous medium two phenomena arise, that have to be taken into account (1) electromigration and (2) electro-osmosis. These two phenomena occur due to the force that an external electrical field exerts on the probe ion, but also on its counter/surrounding ions [7].

Electromigration is the movement of an ion in an electrical field towards the electrode of opposite charge. The velocity at which an ion travels towards its opposite electrode is found by Newton's second law. Newton's second law relates the acceleration of a charged particle to a particular driving force and a drag force. Here the driving force is the Coulomb force and the opposed force is Stokes' drag [12].

$$m\frac{dv}{dt} = qE - 6\pi\mu Rv \tag{1.5}$$

The Coulomb force consists of $q$, the charge of the particle [-], and $E$ the applied electric field [V/m]. Stokes' drag consist of $R$, the radius of the particle [m], $v$, the speed of the particle [m/s] and $\mu$, the viscosity of the fluid [Pa·s]. At zero acceleration, the velocity of a particle immediately follows from eq. 1.5:

$$v = \frac{q}{6\pi\mu R}E \tag{1.6}$$

The velocity attained here is called the drift speed. The drift speed is the velocity that an ion will attend under the influence of a potential gradient. The movement of a particle in an electrical field is not isotropic and the speed, $v$, is proportional to the electrical field, $E$. The proportionality constant between $v$ and $E$, is called the ionic mobility, $\mu_e$ [m²/sV] and equals

$$\mu_e = \frac{q}{6\pi\mu R} \tag{1.7}$$

Substituting eq. 1.7 into eq. 1.6 gives the equation for the drift speed:

$$v = \mu_e E \tag{1.8}$$

The ionic mobility and the molecular diffusion coefficient are related to one another via the Einstein relation eq. 1.9.

$$D_m = \frac{\mu_e K_b T}{Ze} \tag{1.9}$$

Here $D_m$ is the molecular diffusion coefficient$[m^2/s]$, $K_b$ *is* the Boltzmann constant, $1.38{\cdot}10^{23}$ $[J/K]$, $T$ is the temperature $[K]$, $Z$ is the valence $[-]$ and $e$ is the electron charge, $1.6{\cdot}10^{19}$ $[C]$.

Experimental values of the molecular diffusion coefficient of cations are often higher than one would expect based on numerical values of the ionic mobility. This can be explained by electro-osmosis, which arises when an electrical field is applied over a clay sample. Electro-osmosis is the bulk flow of water towards the cathode. It can be explained by the presence of an electrical double layer (Section 4.5) at the charged surface of the porous medium. The negatively charged clay surface is compensated by cations in the pore water. Under the influence of an electrical field, the cations in the double layer move towards the cathode and by viscous drag, a bulk flow of pore water emerges towards the cathode. The electro-osmotic velocity varies linearly with the magnitude of the electrical field [7, 13, 14]:

$$v_{eo} = \mu_{eo} E \tag{1.10}$$

where $v_{eo}$ is the electro-osmotic velocity $[m/s]$ and $\mu_{eo}$ is the electro-osmotic mobility$[m^2/Vs]$.

## 3.2 Mass transport of chemical species

The transport of chemical species can be described by Fick's second law. The accumulation of a species depends on the dispersion of the species and the convection. The dispersion of a species is the combined effect of molecular diffusion and mechanical dispersion. The mechanical dispersion is due to variations in water velocities.

$$\frac{dC}{dt} = D\frac{d^2C}{dx^2} - v_c\frac{dC}{dx} \tag{1.11}$$

Where the first term on the right hand side denotes the dispersion term, with $D$ the dispersion coefficient in $[m^2/s]$ and the second term on the right hand side denotes the convective term, with $v_c$ as the convective velocity.

The convective velocity consists of the two velocities described in the previous section, the electrokinetic velocity and the electro-osmotic velocity, which both depend on the electric field applied. So, $v_c = v_{eo} + v_{em}$.

However, one has to take into account the tortuosity and the retardation of the porous medium when working with clayey soils. Tortuosity is the ratio between the real diffused distance of a particle, *x*, and the experimentally measures end-to-end distance, *z*. The tortuosity is always larger than one.

$$\tau = \frac{x}{z} \tag{1.12}$$

The retardation correction accounts for the fact that probe ions may be sorbed or exchanged etc. (see Chapter 4).

$$R = 1 + \frac{\rho_d K_d}{\eta_{diff}} \tag{1.13}$$

Where $\rho_d$is the dry density of the clay in$[kg/m^3]$, $K_d$ is the distribution coefficient in$[m^3/kg]$, $\eta_{diff}$ is the diffusion accessible porosity [-] and *R* is the retardation factor.

Rewriting the formula for the tortuosity to become $x = \tau z$ and inserting it in Fick's second law eq. 1.12 gives eq. 1.15.

$$\frac{\partial C}{\partial t} = D\frac{\partial^2 C}{\tau^2 \partial z^2} - v_c \frac{\partial C}{\tau^2 \partial z} \tag{1.14}$$

Incorporating the retardation into the equation gives:

$$\frac{\partial C}{\partial t} = \frac{D}{R\tau^2}\frac{\partial C}{\partial z^2} - \frac{v_c}{R\tau^2}\frac{\partial C}{\partial z} \tag{1.15}$$

This can be written as:

$$\frac{\partial C}{\partial t} = D_i \frac{\partial C}{\partial z^2} - V_{app}\frac{\partial C}{\partial z} \tag{1.16}$$

Where τ is the tortuosity [-], $\frac{D}{R\tau^2}$ is the apparent dispersion coefficient $D_i$ in $[m^2/s]$ and $\frac{v_c}{R\tau^2}$ is the apparent convection velocity $V_{app}$ in$[m/s]$.

The superscript 'a, apparent' means: as observed in the porous medium, accounting for tortuosity and retardation.

## 3.3 Deriving the molecular diffusion coefficient

The molecular diffusion coefficient can be derived using the hydrodispersion relationship.

$$D_i = D_{app} + \alpha V_{app} \quad (1.17)$$

The apparent dispersion coefficient and the apparent molecular diffusion coefficient are related via the longitudinal dispersion, $\alpha$ [m], and the apparent velocity, $V_{app}$ [m/s] [7, 9, 13].

To obtain the apparent dispersion coefficient and the apparent velocity, we need to derive an analytical solution for eq. 1.17. With boundary conditions:

*C(z,0) = Qδ(x), C(∞,t) = 0 and C(-∞,t)=0* for *t≥0*

Where Q is the injected activity [Bq] and δ(x) is the Dirac delta function. We obtain:

$$C = \frac{Q}{2S\sqrt{\pi D_i t}} * e^{-\frac{(x-V_{app}t)^2}{4D_i t}} \quad (1.18)$$

With the above equation, one can now fit the experimental data to the calculated data and from this we obtain the $D_i$ and $V_{app}$. Thus, plotting $D_i$ and $V_{app}$ against each other and with eq. 1.18, we can derive the apparent molecular diffusion. The slope of the regression line is the dispersion length and the apparent diffusion coefficient is the intercept with the ordinate axis [7, 14][1].



1. Equation taken from literature. The surface was not included in the original equation.

# 4. Retention processes in clay

Three major mechanisms governing the transport of radionuclides in porous media are diffusion, advection and dispersion. In a suitable clay formation, the radionuclide migration should be diffusion controlled. The most important parameter determining the diffusion is the molecular diffusion coefficient. The diffusion coefficient expresses the speed at which a nuclide travels through clay and is controlled by the sorptive properties of the clay.

Sorption is a general term normally used to cover all aspects of interaction between the mobile phase and the immobile phase. This may include physical and chemical sorption, reduction, filtration and precipitation. In this chapter, we discuss the different sorptive and reduction properties found in clay that influence the radionuclide migration.

This chapter starts with the description of the clay structure in section 4.1. Section 4.2 describes the hydration of clay, followed by an explanation on the cation exchange capacity in 4.3 and anion exchange capacity in 4.4 while section 4.5 handles the electrical double layer and section 4.6 the anions exclusion. The last section explains the influence of porosity on the radionuclide migration.

## 4.1 Structure of clay

The composition of the solid phase and the mobile phase in clay dictates its ability to retard or sorb nuclides. The solid phase and the immobile phase are interdependent and in saturated clays, the compounds in the pore waters and the solid phase are in equilibrium. Saturated clay contains both water in the pores and bound in the interlayer spaces. It is through this water that diffusion can occur.

The solid phase of clay consists of hydrous alumina-silicate groups, where most exist as silicate layers. The silicate layers consist of sheets of tetrahedrally co-ordinated Si and Al atoms (T-sheet) bonded to sheets of octahedrally co-ordinated cations (O-sheet), like $Al^{3+}$ and $Fe^{3+}$. The T-sheets and the O-sheets can form two types of clay minerals: the two-layer type (also known as 1:1-structure or OT-layer) and the three-layer type (also known as 2:1-structure or TOT-layer).

In the 1:1-structure an octahedral sheet is linked to a tetrahedral sheet. In the 2:1-structure an octahedral layer is sandwiched between two tetrahedral layers. The spaces between the layers contain water and the main interlayer cations, which can be any cation, but in practice are $Ca^{2+}$, $K^{+}$ and $Na^{+}$ [15], see Figure 4.

The T-sheet and the O-sheets can be considered the building blocks of all clay minerals. The building blocks make up five main types of clay: kaolinite, illite, vermiculite, smectite and chlorite. Each clay type has it unique chemical and behavioural properties which arises from its specific arrangement [16]. These five main types can be further divided into subtypes.

One of these subtypes is montmorillonite, the main component of bentonite, which is a smectite. Montmorillonite has a 2:1-structure and its main interlayer cations are either $Na^{+}$ or $Ca^{2+}$. $Na^{+}$ and $Ca^{2+}$ can both be well hydrated giving bentonite its ability to swell. See section 4.2 for more information on hydration of clays.

A set of silicate layers and interlayer water form a clay particle. These clay particles are irregularly shaped, cannot be neatly arranged, and are therefore bound to create pores. These pores also contain water and are the main channels through with anions migrated due to the negative surface charge of the clay, see section 4.7.

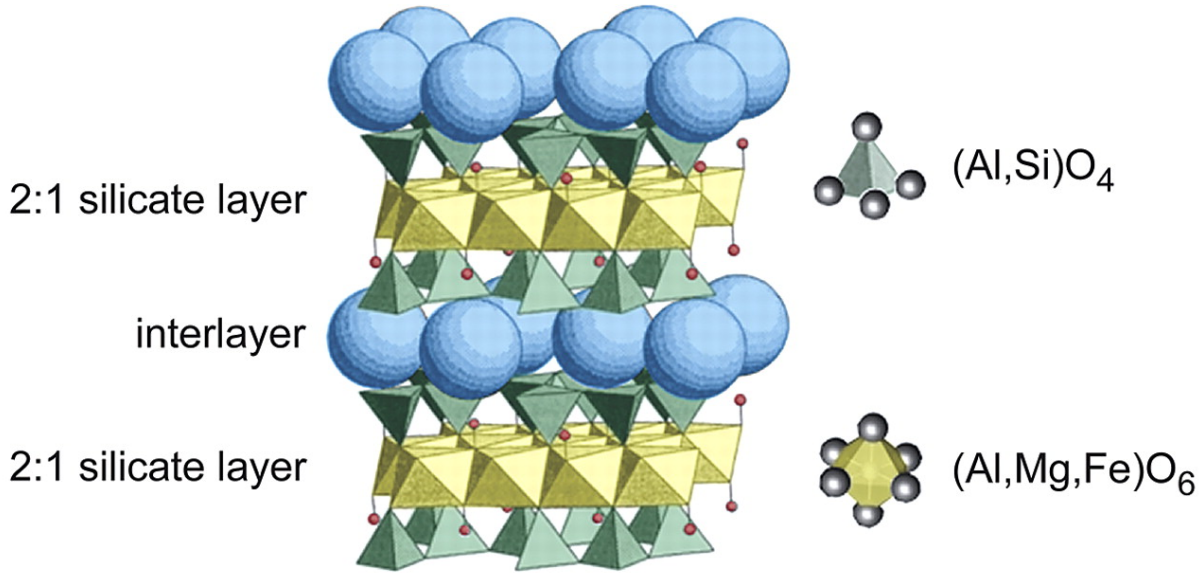


**Figure 3: Schematic representation of a two-layer type clay (also known as 2:1-structure, TOT-layer). The green pyramids represent the tetrahedral silica groups. One silica atom is bond to four oxygen molecules. The yellow double pyramids represent the octahedral elements, this can be Al, Mg or Fe bond to six oxygen molecules The interlayer consist of water molecules and interlayer cations, e.g. $Na^+$ and $K^+$ [17]. The red dots are the oxygen atoms that do not participate in the oxygen crystal and give bentonite a negatively charged surface.**

The oxygen atoms create an oxygen skeleton where the silica tetrahedrals and the octahedrals share oxygen atoms. The octahedrals have two extra oxygen atoms that do not participate in the oxygen skeleton and therefore pointing out of the structure (red dots in the figure 4). These oxygen molecular are the reason the clay negatively charged, see Section 4.5.

## 4.2 Hydration of clays

Clay sheets (i.e. the silicate layers, see Figure 4) in soils are hydrated (surrounded) by water molecules. These water molecules form water layers and hence influence the plasticity, compaction, inter-particle bonding and water movement in clay. These properties change as the thickness of the water layer changes. Water layers and clay sheets bind for two reasons: (1) water is dipolar molecule water and is therefore attracted by the charge on the clay surface (2) the hydrogen ions of water bind to the oxygen atoms in the clay and form a hydrogen bond.

The thickness of the water layers is influenced by two factors: (1) the presence of cations in the solution and (2) the clay surface itself. When a cation is in contact in water, it can become hydrated. When a

cation is in close proximity to the clay surface, it can use water of the clay for its hydration shell. The hydration occurs in steps of one, two and four water layers.

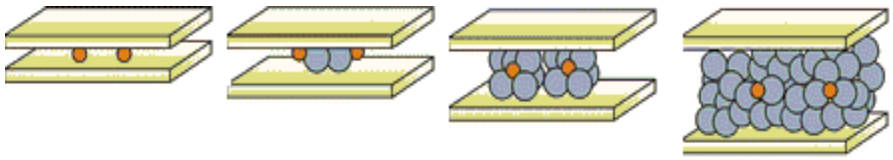

**Figure 4: From left to right the cations are hydrated to different degrees. In outer left picture, the cations are not hydrated. In the outer right picture, the cations are hydrated to a maximum of four water layers. As the water layer tack, the layers show different characteristics. The viscosity of the water molecules in the first layer near the surface is higher than the viscosity of the water molecules located further away [18].**

When water comes near the clay surface, its properties change. Closer to the surface its density becomes higher, when more layers appear the density decreases again. In addition, the viscosity becomes higher; in the first layer, the viscosity may be 100 times higher than that of free water. Lastly, the dielectric constant of water decreases when water comes closer to the clay surface. Water adsorbed by the clay surface can move freely in the direction parallel to the surface but not perpendicular to or away from the surface [15, 19].

## 4.3 Cation Exchange Capacity

To maintain electroneutrality cations from the pore water are bound to the clay particles. The cations that are available to bond to the clay particles are called the exchangeable cations and the quantity of exchangeable cation available is expressed as the cation exchange capacity (CEC) in miliequivalents per 100 gram.

There are two contributing factors to the CEC. The first contribution is independent of pH and electrolyte concentration. It arises from an isomorphous substitution (substitution of one element for another without changing the crystal structure) of Si in the silicate layer by Al (or any other atom with a lower valency e.g. Mg). Al has a lower valency, which creates an excess negative charge in the structure. To compensate for the excess negative charge cations from the pore water are adsorbed onto the surface. The second contribution depends on the electrolyte concentration and is confined to alkaline conditions. When the pH increases the edges of the silicate sheets may become ionised. To compensate for the ionisation cations from the pore waters are adsorbed onto the edges [20].

## 4.4 Anion Exchange Capacity

Anion exchange can be considered the opposite event of cation exchange. The influence of cation is generally much greater than the influence of anions in the majority of soils found in the temperate zones. The influence of cations is especially larger in the three-layer type soils, to which bentonite belongs.

However, in Mica (a clay mineral) for example a positive charge in the soil may originate either from the rupture of sheet of hydrous alumina-silicates units or from the iron and aluminium oxides that cover some crystalline clays (weathering). However, for this thesis the effect of anion exchange may be deemed negligible [21, 22].

## 4.5 Electric double layer

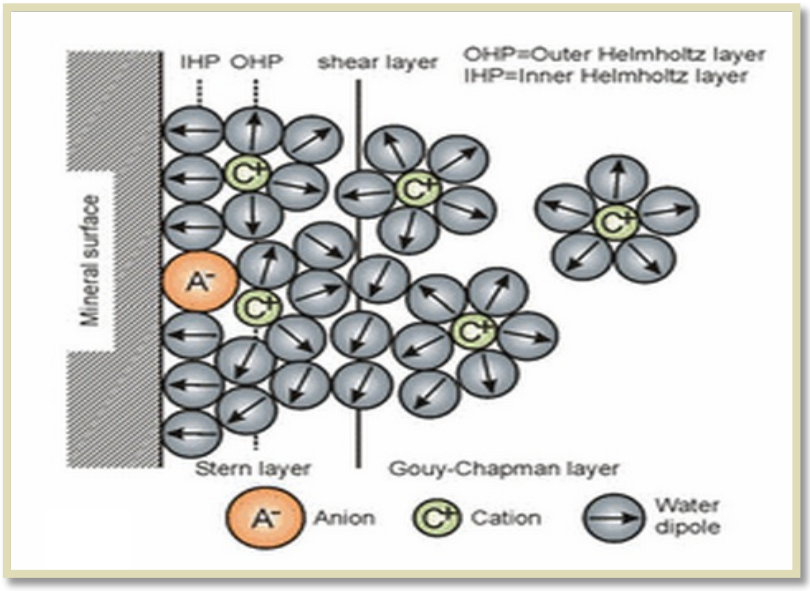


**Figure 5: Configuration of the electrical double layer. In the inner Helmholtz layer the ions are electrically bound to the clay surface. The outer Helmholtz layer contains the opposite ions that are electrically bound to the IHP. Only after the shear layer can the ions be fully hydrated again [14].**

The surface of the clay is negatively charged. To compensate this negative charge, cations from the pore water are drawn to the surface. The double layer refers to two parallel layers that absorb onto the clay surface. The first layer, also called Helmholtz plane, is electrically bound onto the clay surface. The second layer, the diffusive layer, is bound onto the clay surface via coulomb forces, naturally, this attraction is weaker and so this second layer is loosely associated with the surface. It is made of free ions that move in the fluid under the influence of electric attraction and thermal motion rather than being firmly anchored to the clay surface [23, 24].

The electric double layer also influences the hydration of the cations. The cations in the Helmholtz plane are partially hydrated. The Helmholtz region can be divided into an inner layer (IHP) and outer layer (OHP). The plane separating the inner and the outer layer is called the β-plane. The plane separating the outer layer and the diffusive region is called the d-plane. The d-plane is the first plane where cations can exist again fully hydrated [15].

## 4.6 Anion exclusion

Bentonite has a negatively charged surface. This negatively charged surface creates a double layer. The fact that anions and the surface are of the same charge leads to the anion being excluded from the double layer.

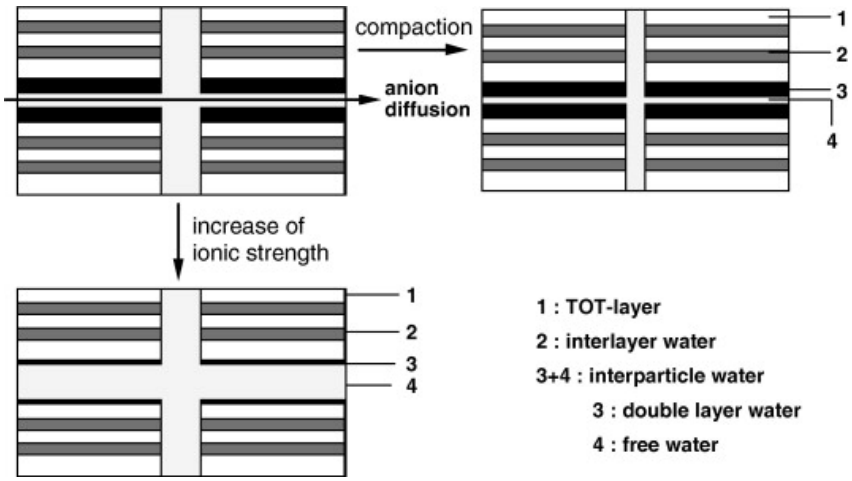


**Figure 6: Influence of compaction and ionic strength on the 'thickness' and 'proximity' of the negative surface charge. Top right) Compaction causes the TOT-layer to lie closer together. Double layer waters lie closer together, increasing negative charge leading to more of anions. Bottom left) Electrolyte of a higher ionic strength decreases the negative charge of the surface leading to less repulsion of anions.**

This effect increases with an increasing charge of the anion. Not only the charge of the anions influences the anion exclusion but also the composition of the pore water in contact with the surface, as well as the compaction of the clay.

A higher ionic strength of the solution results in a better shielding of the negative surface charge, which results in a weaker repulsion of the anions by the charge surface and thus less exclusion[25]. On the contrary, when the clay is compacted the negatively charged surface will be closer to each other and with this increased negative charge the anion will be pushed through faster.

Figure 6 shows the different ways for anions to be excluded. The picture on the left top portraits the initial environment, no increased compaction and no increased ionic strength of the electrolyte solution. The picture on the top right shows an increased compaction. The anions exclusion effect will be stronger as the negatively charged surface lie closer together. The repulsion that the anions than feel will be larger, causing the anions to migrate faster. The picture on the left bottom shows the clay when it is saturated with a solution of a higher ionic strength. As a result, the negative charge of the surface will be less present causing the anions to feel less repulsion and therefore the anions will migrate at a slower pace.

## 4.7 Porosity

The space between the pores in bentonite can be subdivided into two types, (1) the interlayer space and (2) the interparticle space. The interlayer space, is the space between the individual mineral layers, see Figure 7. Is it the space that forms between the tetrahedral and octahedral layers (TOT-layers). The interparticle space is the space present between the clay particles. The interparticle space can be further divided into the diffusive double layer water and free water.

Because of the very narrow space between TOT-layers, the double layers in the interlayers overlap giving rise to a larger electric potential and leading to complete anion exclusion, see Section 4.6. The interlayer water thus exclusively contains cations that compensate the permanent charges located in the octahedral layer of the clay. The total concentration of the cations in the interlayer is constant and independent of the composition of the water in the interparticle pore space.

The spaces between the interparticle pores are larger compared to the spaces between the interlayer and therefore the double layer does not extend as far as that they completely exclude anions. As stated in the previous section, increasing the ionic strength of the pore water results is a more compressed double layer further reducing the anion exclusion effect.

Concluding from all said above, it is clear that a distinction between the interlayer space and interparticle spaces should be made. For anions, the interparticle pores are of interest. The interparticle space equals the space accessible for anions at high ionic strength conditions. [15, 25].

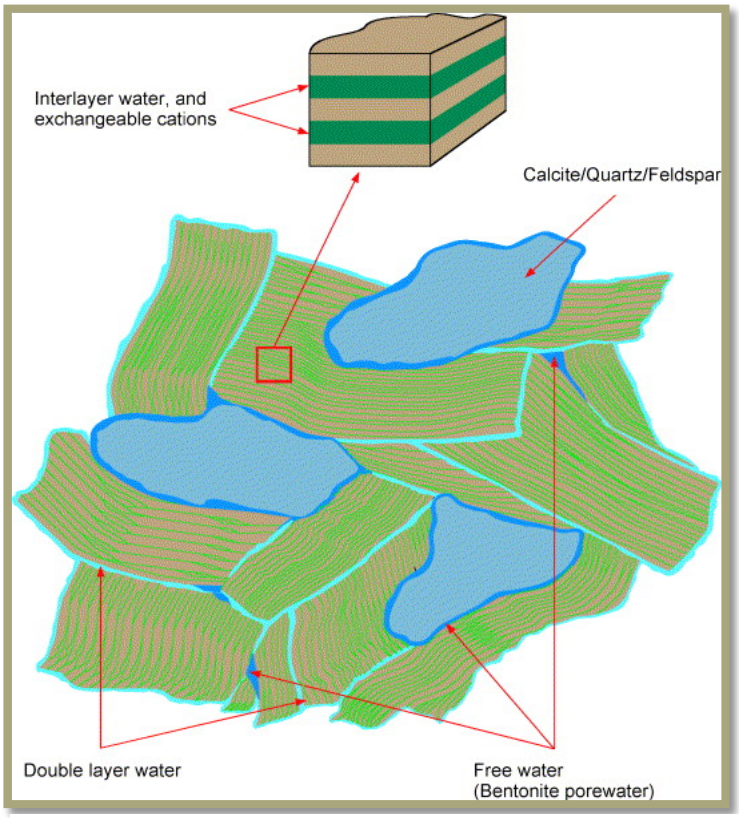


**Figure 7: Schematic overview of bentonite with its pores and double layer water. The double layer has a strong negative charge excluding anions from it. The only migration path they can take is through the free water [3].**

# 5. Geochemical behaviour Ceasium, Technetium and Selenium

## 5.1 Ceasium

Ceasium is a frequently researched isotope and therefore there is an abundance of information available on its isotopes. To determine whether the electromigration cell works properly, we compare data obtained with our electromigration cell to data found in literature, see Chapter 7 for the results.

$^{135}Cs$ and $^{137}Cs$ are the key isotope related to nuclear energy and waste because they are radioactive. $^{135}Cs$ is a long lived isotope, with a half-life of $2.3 \cdot 10^6$ year [26]. $^{137}Cs$ has a half-life of 30 years [26] and is one of two principal medium-lived fission products, next to $^{90}Sr$. Together $^{137}Cs$ and $^{90}Sr$ are responsible for the major part of radioactivity in spent nuclear fuel.

Nevertheless, $^{135}Cs$ is the key Ceasium-isotope in respect to deep geological storage, owing to it long half-life [4]. In this report, we use $^{134}Cs$, a γ-emitter with a half-life of 2 years, to conduct the experiments.

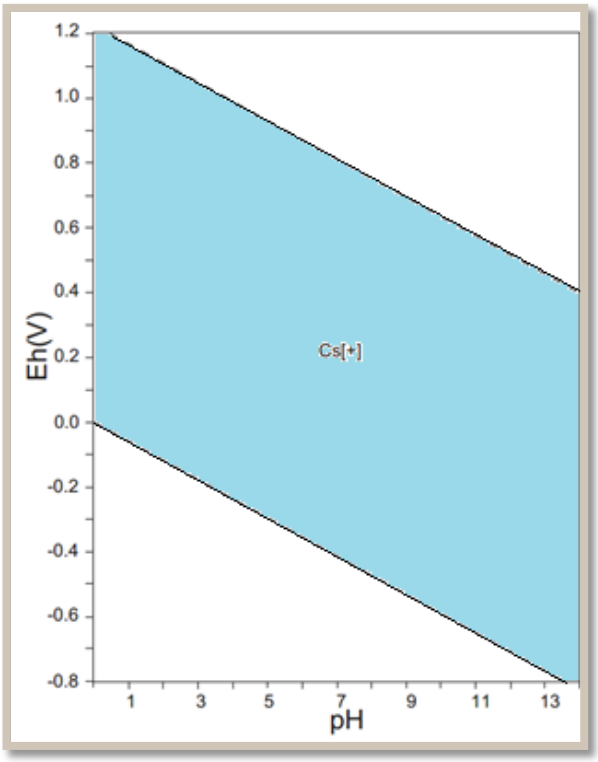


**Figure 8: Speciation of Ceasium in the range of stable water (depicted as the blue plane). Cs has only one oxidation state +1. As a result its speciation is quite simple.**

### 5.1.1 Speciation and oxidation states of Ceasium

Ceasium has simple oxidation chemistry; it has only one oxidation state that is also stable, +1. As a result of its simple oxidation, its speciation in bentonite and all other soils is very straightforward. Ceasium exist as $Cs^+$ at every possible pH and $E_h$.

Figure 8 shows the speciation of Ceasium in the range of stable water. The range of the stability of water is depicted as the blue plane.

### 5.1.2 Retention of ceasium

The CEC, see Section 4.3, gives the largest contribution to the retardation of Ceasium in Bentonite (and other charged soils). The positive Cs-ions are sorbed onto the surface to counterbalance the negative charge of the surface.

A second factor contributing to the retardation of Ceasium in clay is the interlayer collapse of mica-clay. The low hydration energy of Ceasium causes an interlayer dehydration and layer collapse and as a

result the caesium ions are fixed between the clay layers. Thus, the extent to which Cs is retarded depends largely on the CEC of the clay and on the content of Mica in the clay.

### 5.1.3 General migration data of ceasium in bentonite

Published results on the values of $D_{app}$ indicate that the values range from $10^{-9}$ to $10^{-13}$ depending on the clay type (bentonite vs. Boom clay). Sato et al. [27] have conducted migration experiments with Cs on compacted sodium bentonite under atmospheric conditions. The bentonite used (Kunipia-F), contained 95% montmorillinite, which is 10%-higher than the normal montmorillinite content.

Sato et al. found a relationship between the dry density of the bentonite and the apparent diffusion coefficient. As the dry density increases, the $D_{app}$ and the porosity decrease. The retardation does not show a one to one relation to either parameter up to a dry density of $1.4 \cdot 10^3$ [kg/m$^3$]. However, in broad perspective it can be stated that the retardation factor increases with an increasing dry density.

The values for the $D_{app}$ found by Sato et al vary from $10^{-11}$ for bentonites of low dry density to $10^{-13}$ for bentonites of high dry density. Table 1 gives the results as found by Sato et al.

**Table 1: Results as found by Sato et al. An increasing dry density leads to a lower Dapp, an increasing retardation and a decreasing porosity [14].**

| Sample | Dry density [kg/m3] $\cdot 10^3$ | Dapp [m2/s] | Retardation R [-] | Porosity η [-] |
|---|---|---|---|---|
| 1 | 0.2 | $1.6 \cdot 10^{-11}$ | 69 | 0.93 |
| 2 | 0.4 | $1.2 \cdot 10^{-11}$ | 58 | 0.86 |
| 3 | 0.8 | $6.6 \cdot 10^{-12}$ | 62 | 0.72 |
| 4 | 1.0 | $4.8 \cdot 10^{-12}$ | 60 | 0.65 |
| 5 | 1.4 | $2.2 \cdot 10^{-12}$ | 68 | 0.51 |

Tsai, Ouyang & Hsu [28] come to a similar conclusion in their article; with an increasing dry density the values for the $D_{app}$ decrease. For the porosity and the retardation also similar results are found. Table 2 summarises the results found by Tsai et al.

**Table 2: Results as found by Tsai et al. The results show the same trends as the results of Sato et al. [15].**

| Sample | Dry density [kg/m$^3$] $\cdot 10^3$ | Dapp [m$^2$/s] | Retardation R [-] | Porosity η [-] |
|---|---|---|---|---|
| 1 | 1.8 | $2.83 \cdot 10^{-13}$ | 5685 | 0.38 |
| 2 | 2.0 | $1.97 \cdot 10^{-13}$ | 7744 | 0.31 |
| 3 | 2.2 | $1.91 \cdot 10^{-13}$ | 11000 | 0.24 |

In an article by Kim, Suk & Park [29] values for the $D_{app}$ found range from $1 \cdot 10^{-11}$ to $1.13 \cdot 10^{-13}$ . This is in agreement with the results found by Sato et al.

**Table 3: Values found as by Kim et al. The results show similar trends as Sato et al. and Tsai et al. The porosity of the material was not given in the article.**

| Sample | Dry density $[kg/m^3] \cdot 10^3$ | $D_{app}$ $[m^2/s]$ |
|---|---|---|
| 1 | 1.06 | 1.00·10-11 |
| 2 | 1.27 | 7.15·10-12 |
| 3 | 1.58 | 2.57·10-12 |
| 4 | 1.78 | 3.50·10-13 |
| 5 | 1.96 | 1.13·10-13 |

### 5.1.4 Conclusion

Concluding, the main retention process for $Cs^+$ is the sorption onto the clay layer by cation exchange. A smaller fraction of $Cs^+$ may fixated by the interlayer collapse of mica. $Cs^+$ is not reduced by any element or compound in bentonite.

The $D_{app}$ depends on the dry density. The higher the dry density of the grain, the smaller the value for $D_{app}$. Depending on the dry density, values anywhere between $10^{-11}$ and $10^{-13}$ can be found for Ceasium. In addition, the porosity decreases with an increasing dry density. On the contrary, the retardation seems to increase with an increasing dry density.

## 5.2 Technetium

$^{99m}$Tc (half-life of 211·10$^{6}$ a) is like $^{79}$Se and $^{137}$Cs, a long-lived radionuclide and produced as a fission product when $^{235}$U is split in a nuclear reactor. The thermal fission yield is ± 6.1%. Fission of $^{233}$U gives a similar yield of ± 5.1% [30].

Thus far, in the order of tons of $^{99}$Tc have already been produced. Despite the relatively low energy of its radiation - 293,7 keV 99,9984% [31]- its great quantities, long half-life and apparent mobility in soil make it a great concern for long term disposal.

### 5.2.1 Speciation and oxidation states of technetium

Technetium can exist in ions with valences state from -1 to +7, but the most commonly seen oxidation states in natural environments are +4 and +7 [32]. The oxidation state is +7 in oxidizing conditions and +4 in reducing condition.

When Technetium is present in its +7 state, it exists as a pertechnetate anion $TcO_4^-$, and is considered highly mobile and is given a retardation factor of 1. Figure 9 shows that dissolved technetium exist as pertechnetate over the complete pH range, in most oxidizing environments.

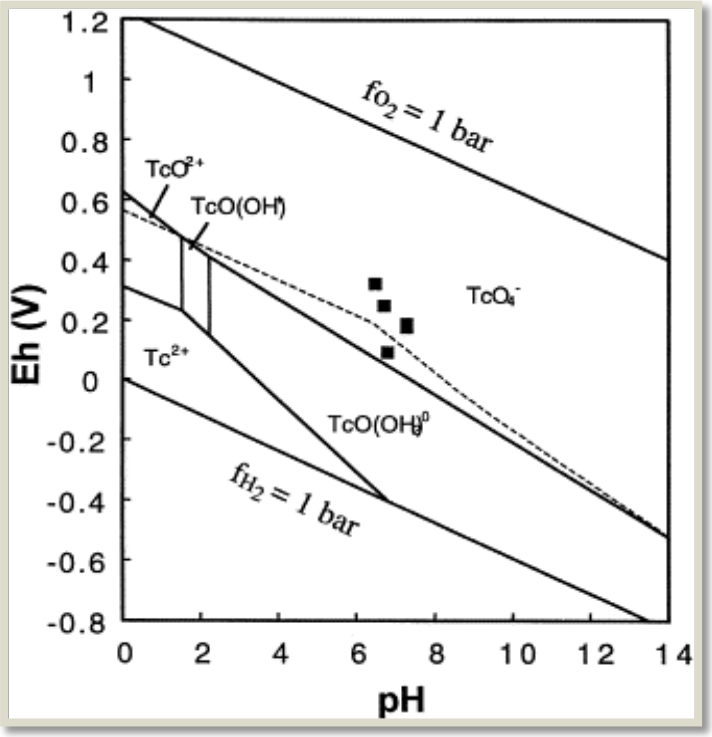


Figure 9: Speciation of technetium [1].

### 5.2.2 Retention of technetium

For soils with low organic material contents, like bentonite, the $K_d$-values (the ratio between the radionuclide concentration in the solid phase to that in the solution) reported for pertechnetate vary between 0 to 0.5 ml/g. The sorption of Tc(VII) has been found to be positively correlated to the levels of organic carbon in soils.

The distribution experiments conducted with Tc show that when the ionic strength is increased the $K_d$-value increases. This is caused by the ionic strength of the solution decreasing the double layer around the sediment particles, allowing Tc to have a higher interaction with the mineral surfaces.

The increase in interaction with the clay surface, increases the chance for the Tc-ion to react with the $OH^-$ for the O-sheets to form the sparingly soluble hydrous oxide that quickly precipitates [33, 34]. Other forms of retention of pertechnetate are physical sorption onto activated carbon [35]. It is also generally accepted that sulphides and Fe(II) reduce Tc(VII) to Tc(IV) and thereby immobilise the Tc-ion through precipitation.

### 5.2.3 General migration data of technetium in bentonite

Although the retardation factor for technetium in a reducing environment is widely accepted as being 1, there are some clues that this might not actually be completely true. In their article Sato et al. conclude that 'a small effect of dry density of bentonite on retardation factor was recognized for $^{90}Sr$, $^{99}Tc$ ,$^{129}I$ and $^{137}Cs$.' They also concluded that the apparent diffusion coefficient of $^{99m}Tc$ decreased with increasing dry density of bentonite. For an overview of the values published by Sato et al., see Table 4. For the apparent diffusion coefficient, values between $6.9 \times 10^{-10}$ and $1.0 \times 10^{-11}$ were found.

**Table 4: Values found for the $D_{app}$ and retardation of pertechnetate in bentonite under oxidizing conditions a)Sato et al [27] and b) Oscarson [36].**

| Dry density x $10^3$ [kg/m$^3$] | 0.8[a] | 1.0[a] | 1.4[a] | 0.9[b] | 1.35[b] |
|---|---|---|---|---|---|
| Dapp [m$^2$/s] | - | $1.3 \cdot 10^{-10}$ | $8 \cdot 10^{-11}$ | $2.3 \cdot 10^{-10}$ | $0.73^{-10}$ |
| Porosity [-] | 0.72 | 0.65 | 0.51 | - | - |
| Retardation [-] | - | 3.2 | 4.5 | - | - |
| $K_d$ [m$^3$/kg] | - | $1.4 \cdot 10^{-3}$ | $1.3 \cdot 10^{-3}$ | - | - |

In an article by Sawatsky and Oscarson [36] similar conclusions were found. An increasing dry density of bentonite decreases the apparent diffusion coefficient. The apparent diffusion coefficient range from $2.3 \cdot 10^{-10}$ [m$^2$/s] at a dry density of $0.9 \cdot 10^3$ [kg/m$^3$] to $8 \cdot 10^{-11}$ [m$^2$/s] at a dry density of $1.4 \cdot 10^3$ [kg/m$^3$].

### 5.2.4 Conclusion

In conclusion, Tc(VII) may be retarded. The retardation depends on the ionic strength of the solution. A higher ionic strength decreases the double layer, allowing the negative Tc-ion to have more interaction with the clay surface. Tc can also be reduced by Fe(II) and sulphides, as well as be precipitated by forming a complexion with $OH^-$. As to which retardation process is more dominant is unclear.

The $D_{app}$ values found lie between $2.3 \cdot 10^{-10}$ [m$^2$/s] and $8 \cdot 10^{-11}$ [m$^2$/s] for respectively low dry densities and high dry densities. A decrease in porosity decreases the $D_{app}$ probably due to the fact that the interparticle pore space is reduced.

## 5.3 Selenium

Among the fission products present in high-level radioactive waste, $^{79}Se$ certainly deserves attention [13]. $^{79}Se$ is a β-emitter with no attendant γ-radiation. The half-life of this radionuclide is uncertain, but is estimated to range between 65000 years and 1.13 million years, the latest figures opt for a half-life of 327000 years [37]. Its yield is set on 0.04%. Despite its low yield, it is present in large enough concentrations that once it escapes from the engineered barrier it contributes considerably to the dose rate to man. Besides that, Selenium is an essential micronutrient for many organisms thus it can be easily bio-concentrated in the food chain [38].

The geochemical behaviour of selenium in clay is controlled by various abiotic reaction, and perhaps microbially-mediated reactions, but due to the high clay compaction, the microbial activity is expected to be very low in bentonite. The main mechanism expected to immobilize $^{79}Se$ in clay are sorption, reduction and precipitation reactions. In the next sections, we will briefly talk about the oxidation states of Selenium, the speciation, the reduction and sorption of Selenium.

### 5.3.1 Speciation and oxidation states of Selenium

The electron configuration of Selenium is given by $3d^{10}\ 4s^2\ 4p^4$ adding up to six electron in its outer shell. This configuration gives selenium its ability to exist in a +1, +2, +4 and +6 oxidation state. Additionally, it can also accept two more electrons given it an extra oxidation state of -2. The most common oxidation states are -2, 0, +4 and +6.

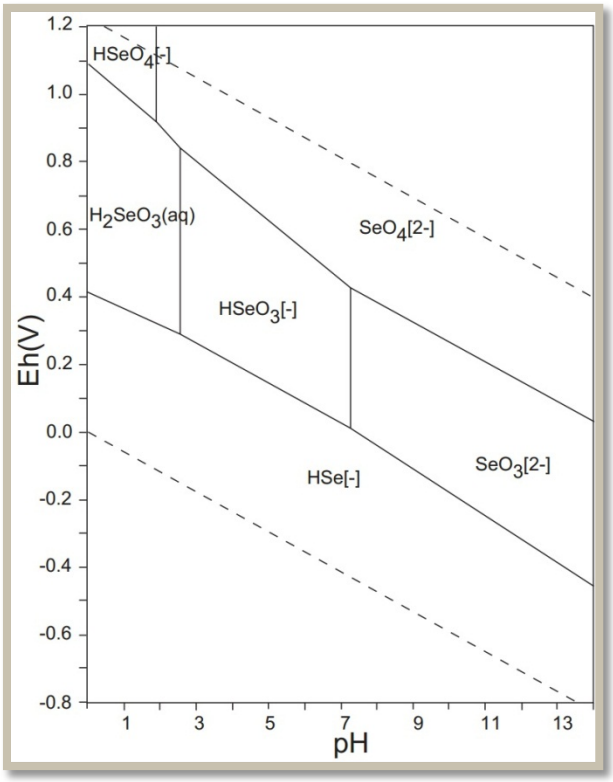


Under mildly reducing conditions, Se(+IV) is the main aqueous species. Under Boom clay conditions (Eh between -450 and -250 mV and pH 8,5), selenium is expected to exist in the form $HSe^-$. However, the oxidation state as it comes out of the nuclear waste matrix is unknown and reduction/oxidation is slow, it might be well possible that it exist in the near field as $SeO_3^{2-}$ and/or $SeO_4^{2-}$ [39].

### 5.3.2 Retention of Selenium

Selenium is always present as an anion in water. The negatively charged surface of bentonite hinders the sorption of the selenium anions. However, some oxyanions can form inner-sphere complexes at the surface of oxy-hydroxides of $Fe^{3+}$ and $Al^{3+}$. This complexation is given in eq. 19 and eq. 20.

$$SeO_3^{2-} + FeOH \leftrightarrow FeSeO_3^- + OH^- \quad (1.19)$$

$$HSeO_3^- + FeOH \leftrightarrow FeSeO_3^- + H_2O \quad (1.20)$$

The iron atoms ($Fe^{3+}$) present in the clay are attracted by the selenite ligands and under the elimination of one hydroxyl group from the clay surface, the selenite takes its place on the surface. The extraction of the hydroxyl group is facilitated in an acidic environment, as the $OH^-$ is rapidly protonated to neutral $H_2O$. The extraction of neutral water is energetically favourable over the extraction of a hydroxyl. The selenite can form a monodentate binding as well as a bidentate binding.

However, as mentioned before the conditions in near field are reducing. Under these conditions, only selenite ($SeO3^{2-}$) forms stable inner-sphere complexes. Selenate sorption is much weaker than that of selenite and requires quite acidic conditions for the ligand exchange. As a consequence, selenate forms preferentially weak outer-sphere complexes and no inner-sphere complexes.

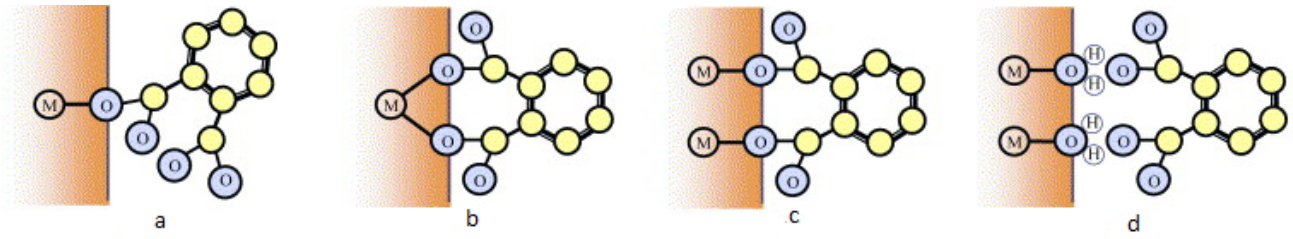


**Figure 10: Schematic of phthalate surface complex structures. a) monodentate inner-sphere complex b) mononuclear (chelating) bidentate inner-sphere complex c) a binuclear (bridging) bidentate inner-sphere complex by both carboxylate groups d) outer-sphere complex.**

Similar to Technetium, selenite (oxidation state +4) is assumed to be reduced by $FeS_2$. For Selenate (oxidation state +6) under Boom clay conditions such a reduction has not been demonstrated and is deemed very difficult in the absence of a catalyst. Kinetic limitation concerning the reduction could be overcome by sulfato-reducing bacteria –SBR-, however these do not exist under Boom Clay conditions [8, 40].

Recent work also mentioned that green rust (Fe(II) hydroxide-sulphate) might be able to reduce selenate in a reducing environment to elemental Selenium, which is considered immobile. Furthermore is Se(-II) is expected to precipitate with $Fe^{2+}$ to form FeSe [41] [42].

### 5.3.3 General migration data of selenium in bentonite

Not much data of selenate in bentonite was found, so values listed in  are values found for selenate in Boom clay. As Boom clay largely consist of bentonite, we believe that it is reasonable to assume that the migration values will be similar to that of bentonite.

The value found for selenite in bentonite is $5 \cdot 10^{-10}$ [$m^2/s$] [43]. The values found for selenate in Boom clay are $1.2 \cdot 10^{-11}$ - $1.7 \cdot 10^{-11}$ [$m^2/s$] [44] and $3.2 \cdot 10^{-11}$ [$m^2/s$] [8]. A small retardation factor of 2.3 was found for selenate in Boom clay.

### 5.3.4 Conclusion

In general, much less information is available on the migration of selenium in bentonite compared we Cs and Tc. However, data was found for the migration of selenium through Boom clay. As Boom clay largely consist of bentonite, we assumed that it is reasonable to compare the migration data of selenium found in Boom clay to that found in bentonite.

Although, selenium is assumed to be unretarded a small retardation factor in Boom clay was found (R=2.3). The retardation is believed to be due to the formation of inner and outer-sphere complexes. Other retention processes are: reduction by $FeS_2$, reduction by green rust and precipitation of FeSe.

Comparing the retention processes of technetium and selenium, there might be competition for the hydroxide of the $Fe^{3+}$ and $Al^{3+}$ octahedrals and for the reduction by Fe(II). Se uses the hydroxides to form inner,- and outer-sphere complexes and Tc uses the hydroxides to be reduced to a insoluble hydrous ion. The competition of Fe(II) is that the iron atom reduce both to a lower oxidation state and thereby immobilizing it.

# 6. Materials and Methods

In this chapter, we describe the details of the experimental set-up, materials and procedures. The technical drawings are given in the Appendices. The electromigration cell was build after example od Bauwers et al [44].

## 6.1 Set-up

The electromigration cell consists of cylindrically shaped sample holder of 10 cm long and 3 cm in diameter with on either side of the sample holder an electrolyte compartment. The electrolyte compartments have a total volume of 100 $cm^3$. Once the sample is secured in its location the sample holder is sealed off from the electrolyte compartments by two glass filters with a diameter of 40 mm and a pore size of 10 µm to 16 µm (VWR- 500-5411). These filters are in place to allow water to flow into the sample but to prevent clay particles from entering the water compartments.

The most important parameter to monitor during the experiment is the electrical field, as the electrical field is the driving force of the experiment. In order to monitor the electrical field, we placed a stainless steel needle every 2.5 cm. These stainless needles can be attached to a volt- and current meter to measure the electric field, see Figures 13, 14 and 15.

The electrolyte compartments are sealed with a lid. On the inside of the lid, we placed coiled stainless steel electrodes with a wire diameter 1 mm. The electrode is connected through the lid to a cable wire that in turn can be connected to the DC-supplier.

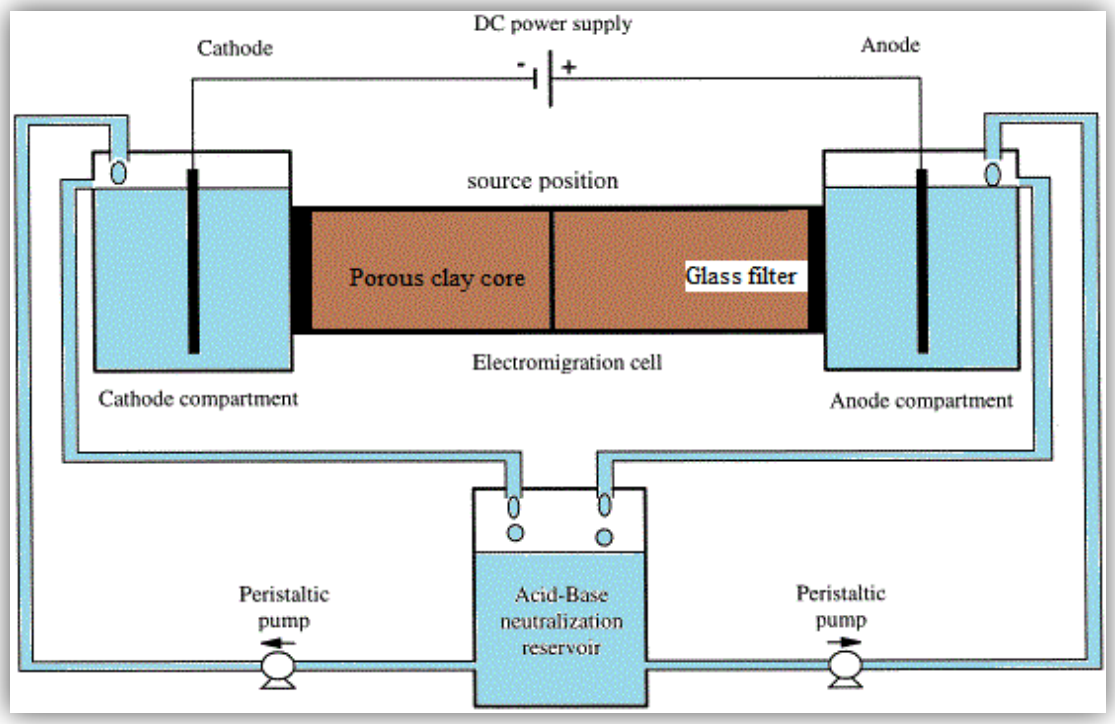


**Figure 11: Schematic overview of the set-up. The cell is connected to a power supply and to two pumps, which are connected to a reservoir. The reservoir has two tubes going back to the cell to refresh the water [2]**

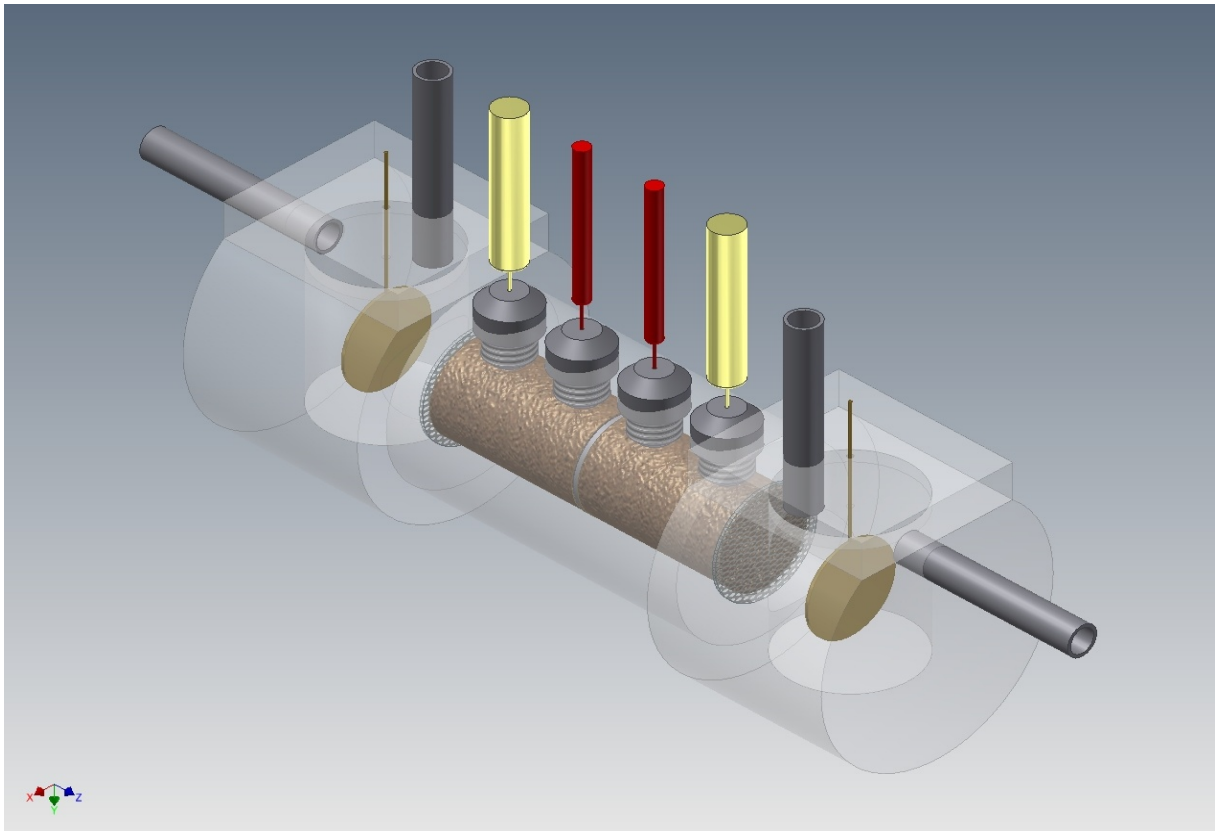

**Figure 12: Technical drawing of the electromigration cell. The electromigration cell is manufactured from a single piece of Plexiglas. The different compartments (sample holders, electrode compartments) were constructed by milling.**

Not only the electrical field influences the experiment, the pH and Eh influence the experiment as well, as it can change the speciation of the nuclide. As the experiment continues the pH and Eh of the experiment change owing to oxygen being produced at the anode and hydrogen being produced at the cathode, see Section 2.3. To monitor the changes a small hole was constructed on top of the electrolyte compartment, wherein a pH meter could be placed (not shown in Figure 12).

When the experiments continue for a longer period (up to a few days) the temperature of the sample could rise. To measure this, four insertions were made on top of the sample holder where thermocouples could be placed. However, when experiments last a day or less the temperature rise is negligible.

The electrolyte compartments proved sensitive to flooding. To solve this problem, two expansion barrels were placed on top of the electrolyte compartments, after which no more flooding occurred, see Figure 13. For a detailed technical drawing of the electromigration cell, see Appendix A.

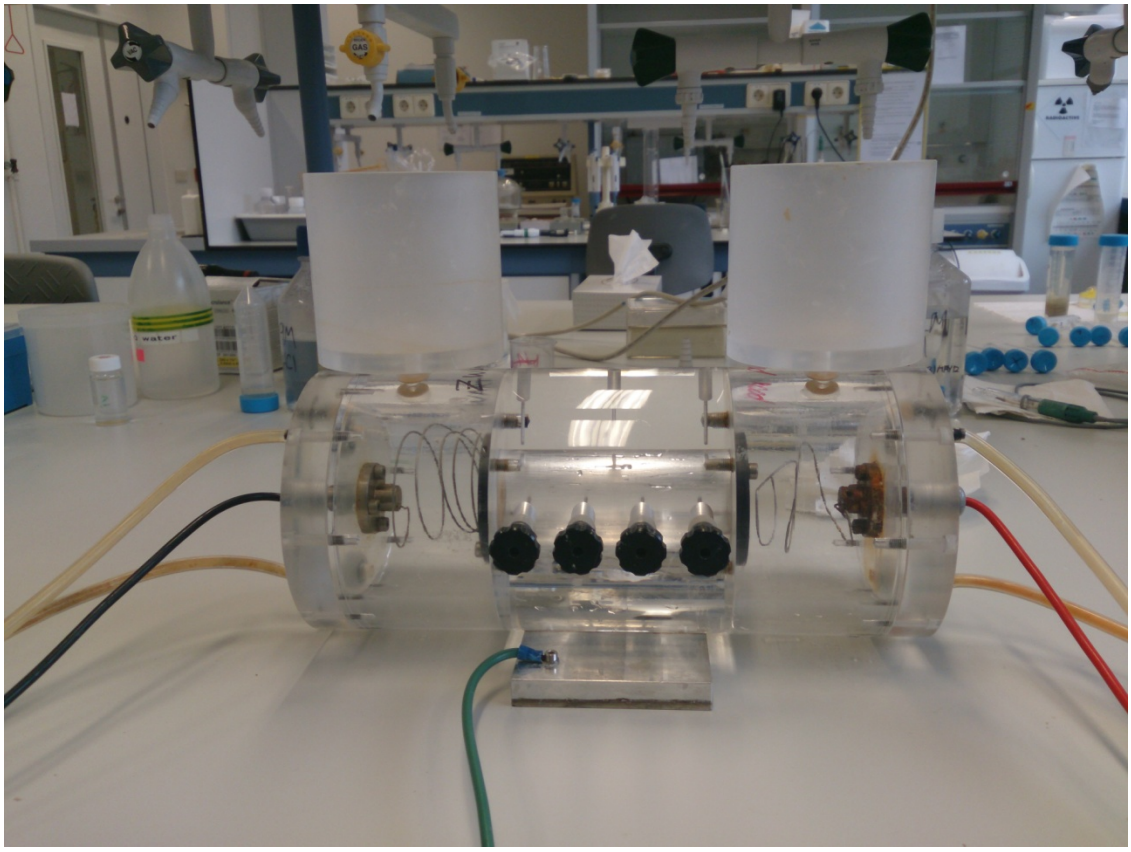

**Figure 13: Picture of the actual electromigration cell. The black and red wires are connected to the power supply. The green wire is to ground the set-up. The four black cloud-shaped elements can be wired to an electrical field meter so that the electrical field over the sample can be measured. The electrodes show a little usage damage.**

## 6.2 Experimental outline

### 6.2.1 Preparation

#### *Isotope production*

*Ceasium*

For the production of 1 MBq $^{134}$Cs (half-life 2yr.) , 10 mg of CsCl containing the stable $^{133}$Cs was irradiated for four hours at the Reactor Institute of Delft with an epithermal neutron flux of $4.45 \cdot 10^{14}$ [1/sm$^2$], a thermal neutron flux of $4.59 \cdot 10^{16}$ [1/sm$^2$] and fast thermal flux of $3.24 \cdot 10^{15}$ [1/sm$^2$]. The irradiated sample was allowed to cool down for two and a half days to let the active chloride decay. The neutron capture reaction of $^{133}$Cs is given in the reaction scheme below:

$$^{133}_{55}Cs + {}^{1}_{0}n \rightarrow {}^{134}_{55}Cs + \gamma \qquad (1.21)$$

As mentioned in Section 5.1, the speciation of Ceasium in rather straightforward, so it will dissolve is any solution. Here, we dissolved the Ceasium in 0.1 M NaOH, so that it would not change the alkaline nature of the synthetic Boom Clay Water.

*Selenium*

Selenium was produced similarly. For the production of 1 MBq $^{75}$Se (half-life 119 days) we irradiated 25 mg of the stable $^{74}SeO_2$ salt for 10 hours (same fluxes as ceasium). The cool down time was similar to Ceasium: two and half days.

$$^{74}_{34}Se + {}^{1}_{0}n \rightarrow {}^{75}_{34}Se + \gamma \qquad (1.22)$$

However, $SeO_2$ is not the compound that we are interested in as it is stable under boom clay conditions. The compounds we are interested in are $SeO_3^{2-}$ (Se +IV) and $SeO_4^{2-}$ (Se +VI). Selenium is often found in redox disequilibrium and due to the unknown oxidation state once it escapes from the waste matrix states $SeO_3^{2-}$ and $SeO_4^{2-}$ might exist if their reduction is kinetically hindered [8].

To obtain $SeO_4^{2-}$ and $SeO_3^{2-}$ we treated $SeO_2$ using 30% W/V $H_2O_2$ and NaOH respectively. The dissolving $SeO_2$ required a bit of stirring [45, 46]

***Making of a technetium generator.***

The production of technetium was slightly more complicate compared to the production of ceasium and selenium. The method used to produce radioactive technetium was through a neutron-gamma reaction of molybdenum. To obtain the technetium, molybdenum was irradiated to serve a technetium generator. For this, we irradiated 50 mg of $^{98}Mo$ for 20 min to produces $^{99}Mo$. The freshly irradiated molybdenum was left to cool down for a day. After this $^{99m}Tc$ could be extracted from the technetium generator.

The reaction scheme of $^{98}Mo$ is given is the equation 1.23. The addition of a neutron to $^{98}Mo$ is followed by γ- emission yields $^{99}Mo$. Through β-emission, $^{99}Mo$ decays to $^{99m}Tc$ (half-life 6 hr.) which in turn decays by γ-emission.

$$Mo^{98}(n,\gamma)Mo^{99} \xrightarrow{\beta-} Tc^{99m} \xrightarrow{\gamma} Tc^{99} \qquad (1.23)$$

Before the separation, the Mo/Tc-mixture was dissolved in hydrochloric acid. Then, the solution was heated on a hot plate at 65 degrees until all the chloride was evaporated and the solution had turned colourless. To speed up the process, the solution was stirred in dry air. The solution was subsequently mixed with 1 M HCl.

The separation of Tc and Mo was carried out by an ion-exchange chromatograph. For the chromatography, a Dowex-1 200-400 mesh was used. The resin was pre-treated with HCL. Then, the syringe was filled with the Dowex and the Mo/Tc-mixture and the solution was pushed gently through a filter. The solution and the filter were then analysed for Mo and Tc present. When the filter contained a fair amount of Mo, the solution was pushed through the filter again until a clean filter was obtained.

Once all the Mo had been removed from the filter. A second filtration was done to wash out the Technetium with 5 ml of 4 M $HNO_3$ [47]. This resulted in a 99,99% pure eluent of technetium.

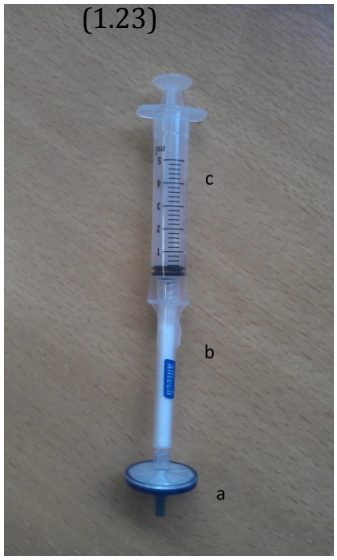


**Figure 14: The Technetium generator. a) a 2 micron filter. b) a small syringe filled with Dowex-1 200-400 pretreated with HCL. c) a 5 mL syringe that can be filled with the Mo/Tc-mixture that is dissolved in HCl.**

*Recipe for Synthetic Boom Clay Water*

The main component of Boom clay pore water (BCW) is $NaHCO_3$ in addition there are some minor fractions of other components like Boric acid. Thus, basically, BCW is a 15 mM $NaHCO_3$ solution. If one wants to make synthetic Boom Clay Water (SBCW), one could use a 15 mM $NaHCO_3$ solution. However, at the SCK·CEN scientists issued a detailed recipe to make synthetic boom clay water (SBCW).

The recipe can be found in appendix B. In order to work with SBCW in an anaerobic environment, the water should degassed by bubbling it through with N or Ar overnight and leave it open in an inert glove box [48].

*Sample preparation*

To obtain clay samples that were as homogeneous as possible, small Plexiglas tubes of 10 cm long and a diameter 3 cm were made. The tubes were filled with bentonite and sealed off with a porous filter on both ends. The tubes were placed into SBCW and left to rest until the powder was saturated (approximately two months).

A faster method was to fill the electromigration cell with powder and to start the set-up. The electrical field forces the water to travel through the powder, this way the samples were saturated within four/five days. The saturation was checked by determining whether the electrical field over the sample stopped changing.

The fasted method was to mix equal amounts of water and bentonite manually. The clay had to be kneaded thoroughly to obtain a sample as homogenous as possible. The kneaded clay was then moulded into two 5 cm long Plexiglas tube with a 3 cm diameter.

### 6.2.2 Experimental procedure

Once the SBCW, isotope solutions and clay samples were prepared, the set-up was filled with two clay cores of each 5 cm. The first clay core was placed into the set-up after which we place a small round piece of filter paper on top of it. The filter paper was wetted with a small amount of SBCW, 36 µl, and then with the active solution. For a ceasium and selenium test, we typically used between 150 and 250 kBq and for technetium test we typically used 1 MBq.

After the filter paper was spiked, we placed the second clay core on top and closed the exit with the glass filters. Hereafter, we filled the electrolyte compartments with the SBCW and started the experiments.

As constantly monitoring devices were not available, we listed the electric field, the voltage, the pH and Eh every hour. The electric field might change as the experiments proceeded due to precipitation at the electrodes. When this happened, it is needed to adjusted the current to maintain a constant electric field. The data could not be listed overnight , thus the experiments were stopped at the end of a working day and continued the next day.

After a cycle, the samples were removed from the cell and cut it in slices of 4 mm with a knife. These slices were put into plastic vials of 40 ml and 40 ml of Mili-Q water was added. The vials were shaken overnight on a rotator.

The next day, 2 ml of the shaken sample solution of each vial was transferred into glass vial suitable for a Wizard 2 automatic gamma counter (Wallace). Then, the vials were ran through the detector.

To determine the dry density, we first needed to determine the grain density. The following steps were taken to obtain the grain density[49]. We dried 15 gram of clay samples at $105^0$C for 24 hour in a ventilated oven to remove adsorbed water. Then, the samples were taken out of the oven and quickly poured into a volumetric flask, which was then sealed and let cool to room temperature. We then added 35 ml (or sufficient liquid) of 1 M to the flask, until the sample was completely covered. Then, the flask was sealed again.

After this, we shook and rotated the sample for some time (typically one hour) to facilitate the air from escaping the bentonite. Next, the samples were left to rest for 24 hours before they were rotated again and filled with the rest of the 1 M NaOH until the flask was full. The last step was to weight the flask, the test liquid and the bentonite together. For the experimental recipe, see Appedix D.

The grain density was determined using the following equation:

$$D_s = \frac{m_s}{V_{tot} - \frac{m_{tot} - m_{s+f}}{D_l}} \quad (1.24)$$

where $m_s$ is the mass of the solid (clay sample after drying) [kg], $V_{tot}$ is the total volume [$m^3$], $m_{tot}$ is the total mass, $m_{s+f}$ is the mass of the solid and the flask [kg] and $D_l$ is the density of the liquid [kg/$m^3$].

Once the dry density was determined, we could calculate the dry density through the following equation:

$$D_d = \frac{D_s \cdot D_w}{D_s \cdot w + D_w} \quad (1.25)$$

Where $D_s$ is the grain density [kg/$m^3$], as calculated above, $D_w$ is the density of water [kg/$m^3$] and w is the water ratio [-] and is calculated by:

$$w = \frac{m_w}{m_s} \quad (1.26)$$

where $m_w$ is the mass loss due to drying the sample at $105^0$ C for 24 hours and $m_s$ is the remaining solid mass.

### Data processing

The detector measures the absolute activity that is found in each slice. For each series, we normalized the data by dividing the activity of a slice through the slice with the most activity. Then each normalized slice received a location on the x-axis, so that distance travelled could be determined.

To obtain the dispersion coefficient we wrote a program in Matlab that could fit the experimental data to the calculated data, using the equation below:

$$C = \frac{Q}{2S\sqrt{\pi D_i t}} e^{\frac{\left(x - V_{app} t\right)\hat{}2}{4 D_i t}} \quad (1.18)$$

where Q is the initial concentration or activity [Bq], S is the surface [$m^2$], $D_i$ is the molecular dispersion coefficient [$m^2/s$], t is the time [s], x is the distance [m], $V_{app}$ is the apparent velocity [m/s] . See Chapter 3 for the derivation. All parameters are known except for the dispersion coefficient that has to be fitted, but here we also fitted the apparent velocity. The Matlab script can be found in Appendix C.

Once the dispersion coefficient was obtained for the different experiments, the dispersion coefficients were plotted against the apparent velocity of those experiments and from that, we obtained the apparent molecular dispersion coefficient and the longitudinal length. The apparent molecular diffusion coefficient is the value where the regression line crosses the y-axis.

$$D_i = D_{app} + \alpha V_{app} \quad (1.14)$$

The accuracy of the fits was reviewed by a part of the code that calculated the sum of squares.

To calculate the retardation, the solid grain density, the dry density [49] had to obtained and the porosity [50] had to be calculated first using eq. 1.27:

$$\varepsilon = 1 - \frac{\rho_d}{\rho_s} \quad (1.27)$$

where ε is the total porosity [-], $\rho_d$ is the dry density [$kg/m^3$] and $\rho_s$ is the solid grain density [$kg/m^3$].

With the porosity and distribution coefficient obtained from literature the retardation was calculated using the equation below [28]:

$$R = 1 + \left(\frac{1 - \varepsilon}{\varepsilon}\right) \rho_s K_d \quad (1.24)$$

Where $R$ is the retardation [-], $\varepsilon$ is the total porosity [-], $\rho_s$ is the solid grain density and $K_d$ is the distribution coefficient in [ml/g].

# 7. Results and discussion

## 7.1 Ceasium

Twelve experiments with Ceasium were conducted, five of the experiments were omitted due to experimental mistakes e.g. the location of the spiked tracer was unknown, flooding and overheating of the pump and due to the tracer not leaving the origin. With the remaining experimental data, a distribution profile was obtained. The experimental distribution profile was then fitted to a calculated distribution profile with MATLAB. With that, the dispersion coefficient and apparent velocity could be obtained. The sum of square –SS- was also calculated to determine the accuracy of the fit. The results of the fitting and the experimental relevant data are listed in Table 5.

Table 5: Results found in the experiments done during the electromigration experiments with Ceasium

| Experiment code | Time [hr] | Electric field [V/m] | $pH_{cathode}$ | $D_i$ [$m^2/s$] | $V_{app}$ [m/s] | Current [mA] | SS |
|---|---|---|---|---|---|---|---|
| **Cs-1** | 18.5 | - | 8.3 | 1.65E-10 | 2.10E-07 | 10 | 0.081 |
| **Cs-2** | 11.5 | - | 9,4 | 1.60E-10 | 2.66E-07 | 15 | 0.077 |
| **Cs-3** | 12.75 | - | 9,8 | 2.10E-10 | 3.70E-07 | 17 | 0.068 |
| **Cs-4** | 13 | - | 9,7 | 1.48E-10 | 1.39E-07 | 13 | 0.049 |
| **Cs-5** | 7.25 | 64 | - | 1.40E-10 | 2.68E-08 | 40 | 0.042 |
| **Cs-6** | 6 | 71 | 7.3 | 1.70E-10 | 5.56E-08 | 35 | 0.042 |
| **Cs-7** | 6.5 | 46 | 9.3 | 1.08E-10 | 2.56E-08 | 25 | 0.049 |

The aim was to investigate if experimental time could be reduced to a few hours. The distribution profiles obtained are promising. The experiments that were done for a shorter period of time (and at a higher velocity) all show a typical Gaussian profile except for experiment Cs-6, the shortest experiment. Experiment Cs-6 shows some tailing, this could be due to the reduced experiment time that did not allow all tracer to leave the origin. However, experiment Cs-6 had the highest applied electrical field and since the experiments Cs-5 and Cs-7 do not show such tailing, it is believed that the tailing is caused by contamination during the cutting of the slices.

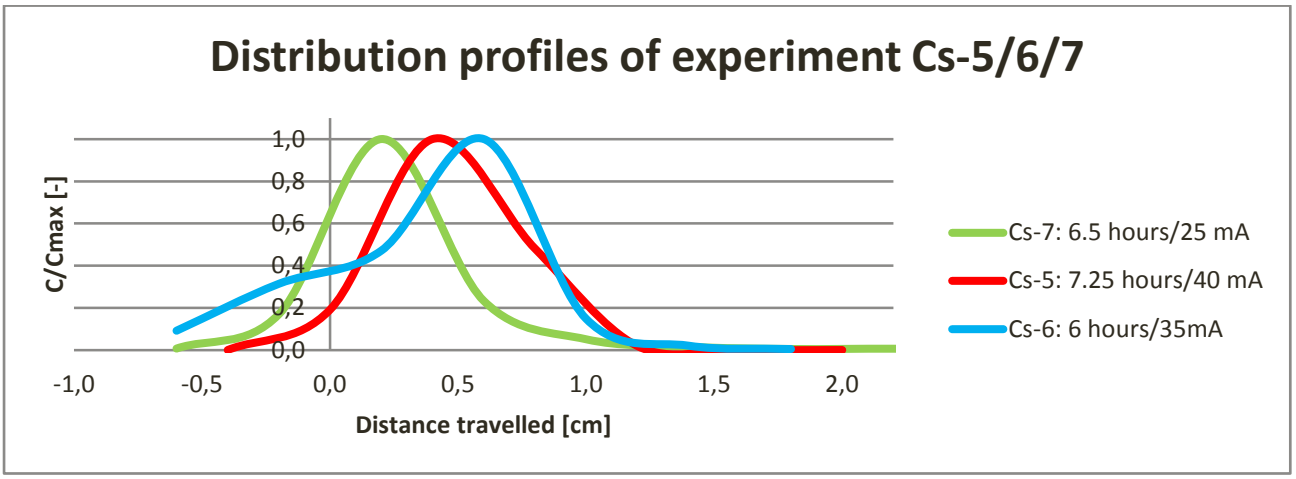


**Figure 15: Migration profiles obtained during high current experiment conducted with an electromigration cell in Clear Gaussian distribution profiles are obtained. Prove that eperimental time can be further reduced. electromigration experiments.**

Based on the current experiment Cs-5 would have travelled the largest compared to experiment Cs-6, this is however not the case. The explanation can be found in the electric field over the sample. Although, experiment Cs-5 had the largest current applied the electric field is smaller than the electric field in experiment Cs-6. This due to the precipitation of rust at the electrodes.

In the experiments, we used SBCW. The SBCW contained minor fraction of Fe(II) which oxidised during experiments and formed rust. During experiment Cs-5, the rust formation was more severe than in experiment Cs-6 changing the overall resistance and hence lowering the electrical field over the sample. With the driving force reduced the distance travelled was less.

The production of rust proved troublesome as it influenced the electrical field applied and damaged the electrodes. The electrode at the cathode was affected to such a degree after the first set of experiment it broke down and had to be replaced. It was then decided to omit Fe(II) from the SBCW in future experiments.

Once the dispersion coefficient and apparent velocities of the experiments were set out against each other, it became evident that two lines were present. One line for the low current experiments (20 mA and lower) and for the high current experiment (25 mA and higher). (Figure 16 gives a distorted image of the slope of the high current experiments due to the scale on the x-axis).

The two trend lines give both a more or less similar apparent molecular diffusion coefficient. Thus is it is definitely possible to shorten the experimental time. However, it is not possible to mix higher current and low current experiments, thus far. Not only because the apparent velocities lie greatly apart but also because the dispersion at high current experiments is more severe.

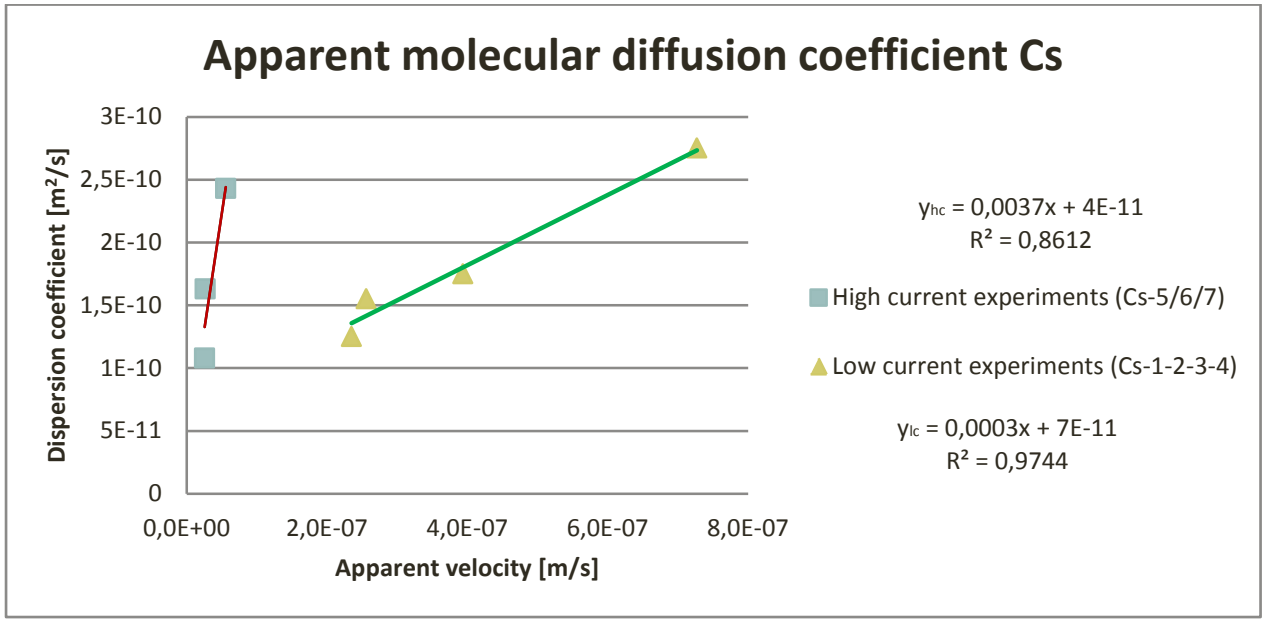


**Figure 16: apparent velocity on the x-axis plotted against the dispersion coefficient on the y-axis. Two trends are visible for the experiments conducted at high current and at low current.**

Looking at the longitudinal dispersivity obtained, it is clearly noted that the longitudinal dispersivity between the high current experiments and the low current experiments differ by one order of a

magnitude ($3.7 \cdot 10^{-3}$ [m] vs. $3 \cdot 10^{-4}$ [m]). This can be explained by the fact that during a high current experiment the water velocities through the clay are higher. Longitudinal dispersivity quantifies how

much a radionuclide (or particle more generally) strays away from the path of the ground water in which it is carried. When a radionuclide travels into a dead end pore or another diverting path it will get behind the average velocity more rapidly, causing a greater spread in the longitudinal direction.

The apparent velocities obtained are $4 \cdot 10^{-11}$ [$m^2/s$] and $7 \cdot 10^{-11}$ [$m^2/s$] for the high and low current experiments respectively. The order of a magnitude raises the suspicion that the bentonite used was one of a low dry density. Experiments conducted on the dry density of the bentonite indeed show that the bentonite had a relatively low dry density of $0.9 \cdot 10^3$ [$kg/m^3$].

**Table 6: Comparison of data found in this experiment with data obtained by Sato et. al [27] and Kim et al. [29].**

| | Our data | Sato et al. | Sato et al. | Kim et al. |
|---|---|---|---|---|
| **$D_{app}$ [$m^2/s$]** | $4\text{-}7 \cdot 10^{-11}$ | $6.6 \cdot 10^{-12}$ | $2.2 \cdot 10^{-12}$ | $1.0 \cdot 10^{-11}$ |
| **Porosity [-]** | 0.50 | 0.72 | 0.51 | - |
| **Dry density [$kg/m^3$] $\cdot 10^3$** | 0.9 | 0.8 | 1.4 | 1.0 |

Comparing the $D_{app}$ based on dry density, the results found are in good agreement with the results found by Kim et al. However, comparing the results with Sato et al. we see that the order of magnitude is lower.

Thus, comparing the data to Kim et al, we can conclude that the experiments were successful. The range of base is not unreasonably large. Each batch of bentonite may vary in CEC and montmorillinite content. The natural variation is the clay cannot be neglected and may influence the results.

However, compared to Sato et al. we cannot definitely state that the experiments were successful. The difference in magnitude could be caused by the preparation of the clay sample. We mixed the bentonite clay in a 1:1 ratio with water and kneaded the clay thoroughly, however, it cannot be excluded that can channels existed in the clay sample or that the clay was not completely saturated. To avoid this in future experiments we design a tube wherein the bentonite powder could be placed and left to rest until saturation (see Chapter 6).

## 7.2 Technetium

Figure 17 shows the concentration profiles of $^{99m}Tc$ as they were obtained during the electromigration experiments. The distribution profiles are obtained in a similar manner to Ceasium. The concentration of the technetium was normalized to the maximum amount of activity found in one of the slices of the sample. The x-axis is chosen such that the direction in which the nuclide travel is positive. In this case, that is towards the anode.

As $^{99m}Tc$ is a short lived isotope, it is interesting to determine whether experimental time can be reduced into a time span that is suitable to conduct experiments with short lived isotopes. In the shortest experiments, experiments 2 and 3, a typical Gaussian diffusion profile was observed after only 3 hours. Some activity remained in the origin but the peak position is clearly located away from the origin, so a data can be extracted from the distribution profiles.

The other experiments lasted longer but at a lower current. It can be seen from the graph that with these experiments the peak position is located even further from the origin. Which is more desirable as it is more convenient to determine the peak.

Compared to the Cs-experiments the experimental time for Tc can be reduced even further. Only after three hours did we obtain a typical Gaussian profile(after 5 hours most activity remained in the experiments conducted with Cs). Ceasium is more retarded in bentonite; hence did we need a longer period to obtain a Gaussian profile located away from the origin.

In this set of experiments, we also experience troubles. Although, we excluded Fe(II) from the SCBW we had serious formations of acid and alkaline fronts in the electrolyte compartments. This required us to constantly adjust the pH and Eh to maintain the right speciation of Technetium. The pH and Eh changes also appeared in the Cs-experiments, but as the speciation of Cs is simple changes in pH and Eh do not affect its chemical form.

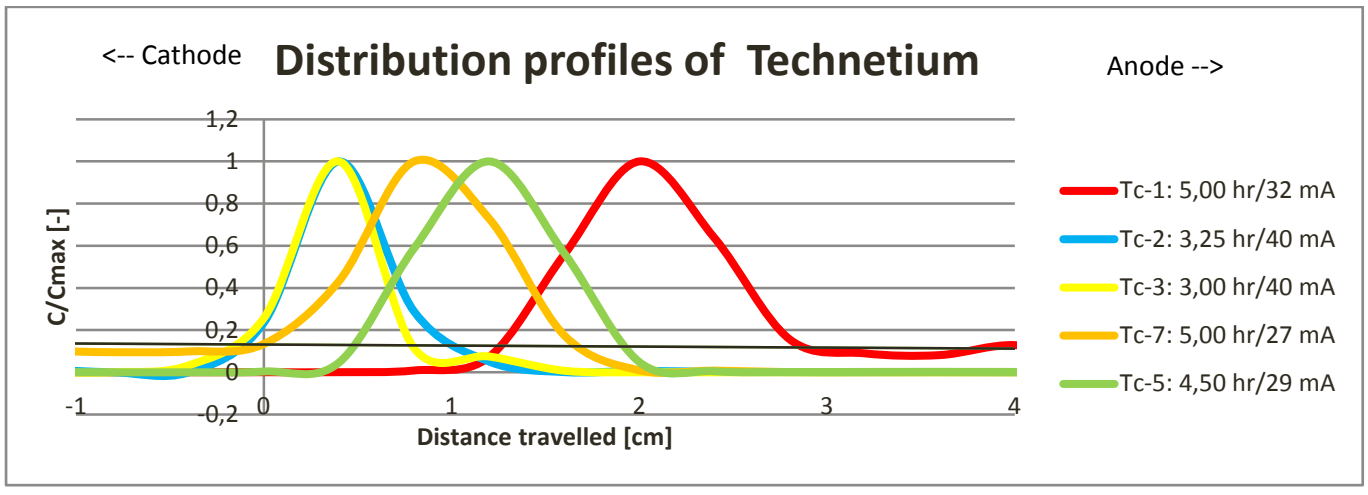


**Figure 17: Migration profiles obtained during electromigration experiments in water-saturated Na-bentonite with a dry density of $0{,}3 \cdot 10^3$ kg/m$^3$ at room temperature**

As no abnormal patterns were observed in the distribution profiles of the Technetium experiments. So next, we determined the apparent molecular diffusion coefficient of technetium by fitting the experimental data in Matlab to obtain the $D_i$ and $V_{app}$. The results are given in Table 6. Experiment 6 was omitted due to the fit not being accurate enough –sum of squares was ≈ 0.2-.

Table 7: results of the experiments done with $^{99m}Tc$

| Experiment code | Time [hr] | Electric field [V/m] | $pH_{cathode}$ | Eh [mV] | $D_i$ [$m^2/s$] | $V_{app}$ [m/s] | Current [mA] | SS |
|---|---|---|---|---|---|---|---|---|
| **Tc-1** | 5 | 55 | 8.3 | -81 | 4.25E-10 | 1.11E-06 | 30 | 0.043 |
| **Tc-2** | 3.25 | 71 | 8.4 | -18 | 2.55E-10 | 3.42E-07 | 40 | 0.004 |
| **Tc-3** | 3 | 72 | 8,8 | -17 | 2.45E-10 | 4.04E-07 | 40 | 0.017 |
| **Tc-5** | 5 | 48 | 7.4 | -76 | 3.95E-10 | 9.44E-07 | 29 | 0.080 |
| **Tc-7** | 4.5 | 51 | 8.5 | -85 | 4.05E-10 | 7.40E-07 | 27 | 0.067 |

With this set of data, the $D_{app}$ was obtained by plotting the apparent velocity against the dispersion coefficient once again.

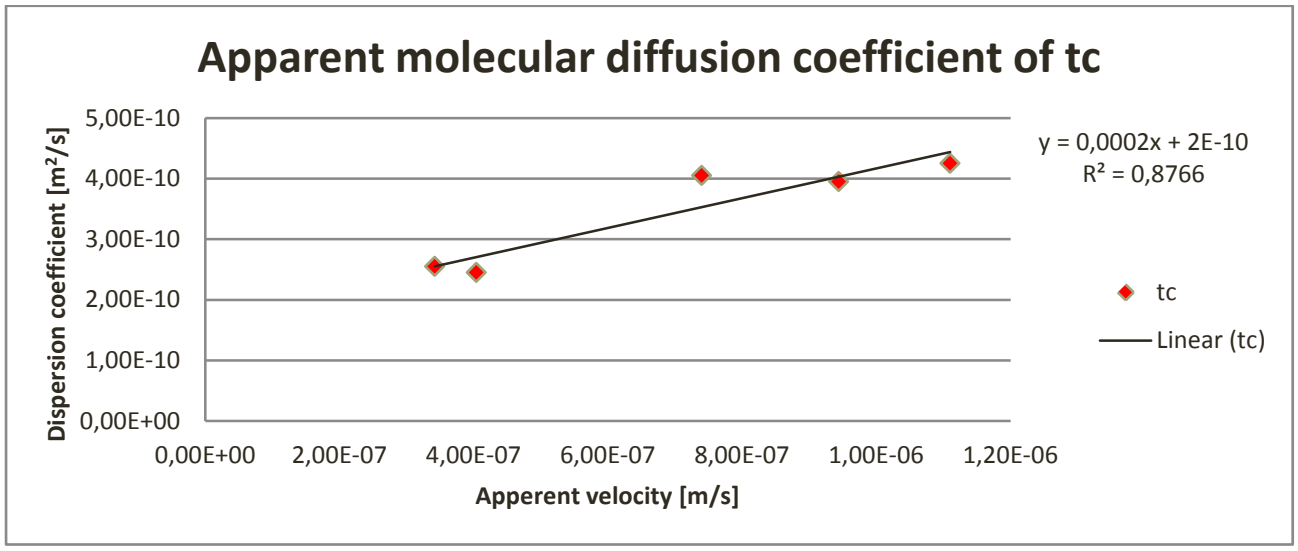


Figure 18: The apparent velocity and dispersion coefficient of the Tc-experiments plotted against each other.

The dispersion length value is $2 \cdot 10^{-4}$ [m]. In other research values between $10^{-3}$ [m] and $10^{-4}$ [m] are found [7]. However, the most important parameter is the apparent molecular diffusion coefficient. The $D_{app}$ obtained is $2 \cdot 10^{-10}$ [$m^2/s$] at a dry density of $0.9 \cdot 10^3$ [$kg/m^3$]; this is in good agreement with results found in literature. Sato et all. obtained in their research a $D_{app}$ of $1.3 \cdot 10^{-10}$ [$m^2/s$] at a dry density of $1.0 \cdot 10^3$ [$kg/m^3$] and Oscarson found a $D_{app}$ of $2.3 \cdot 10^{-10}$ at a dry density of $0.9 \cdot 10^3$ [$kg/m^3$].

Table 8: Apparent diffusion coefficients and retardation factors at different dry densities. [a]Sato et al. [b]Oscarson. [c1] Out value retardation calculated with $K_d$ -values of 0.0014 [ml/g] [c2] retardation calculated with $K_d$ -value of 0.0013 [ml/g].

| Dry density x $10^3$ [kg/$m^3$] | 0.8[a] | 1.0[a] | 1.4[a] | 0.9[b] | 0.9[c1] | 0.9[c2] |
|---|---|---|---|---|---|---|
| Dapp [$m^2$/s] | - | $1.3 \cdot 10^{-10}$ | $8.0 \cdot 10^{-11}$ | $2.3 \cdot 10^{-10}$ | $2 \cdot 10^{-10}$ | $2 \cdot 10^{-10}$ |
| Porosity [-] | 0.72 | 0.65 | 0.51 | - | 0.50 | 0.50 |
| Retardation [-] | - | 3.2 | 4.5 | - | 3.2 | 3.4 |
| $K_d$ [ml/g] | - | $1.4 \cdot 10^{-3}$ | $1.3 \cdot 10^{-3}$ | - | $1.4 \cdot 10^{-3}$ | $1.3 \cdot 10^{-3}$ |

Is this research we found a small retardation factor for technetium. Two retardation factors were calculated, one for a $K_d$-value of $1.4 \cdot 10^{-3}$ [ml/g] and one for a $K_d$-value $1.3 \cdot 10^{-3}$ [ml/g] (eq. 1.10). This to account for the dry density and the porosity. The retardation factors calculated have a value of 3.2 and 3.4.

Thus, some retardation processes are present. No Fe(II) was added to the SBCW, so the retention process could be either the reduction of Tc(+VII) to Tc(+IV) or complex forming with the hydroxyls However, more research should be done to obtain a solid conclusion.

## 7.3 Selenium

Six experiments were conducted with Selenium. In experiments Se-1 and Se-2 the chemical form was selenite and in experiments Se-3 through Se-6 the chemical form was selenate. $SeO_2$ was irradiated and the dissolved in sodium hydroxide and hydrogen peroxide, respectively. The experimental conditions are listed in Table 10.

**Table 9: Experimental conditions under with the selenium experiments were conducted.**

| Experiment code | Time [hr] | Electric field [V/m] | $pH_{cathode}$ | Eh [mV] | $D_i$ [$m^2/s$] | $V_{app}$ [m/s] | Current [mA] | SS |
|---|---|---|---|---|---|---|---|---|
| **Se-1** | 12.5 | 17 | 7.7 | - | - | - | 10 | - |
| **Se-2** | 6.5 | 47 | 7.4 | - | - | - | 30 | - |
| **Se-3** | 6 | 50 | 8.5 | 28 | 1.75E-10 | 2.96E-07 | 27 | 0.038 |
| **Se-4** | 6 | 52 | 7.4 | 80 | 4.45E-10 | 8.89E-07 | 27 | 0.092 |
| **Se-5** | 4.5 | 48 | 9.4 | -25 | 4.40E-10 | 1.17E-06 | - | 0.039 |
| **Se-6** | 9 | 34 | 8.4 | 73 | 3.85E-10 | 6.67E-07 | - | 0.067 |

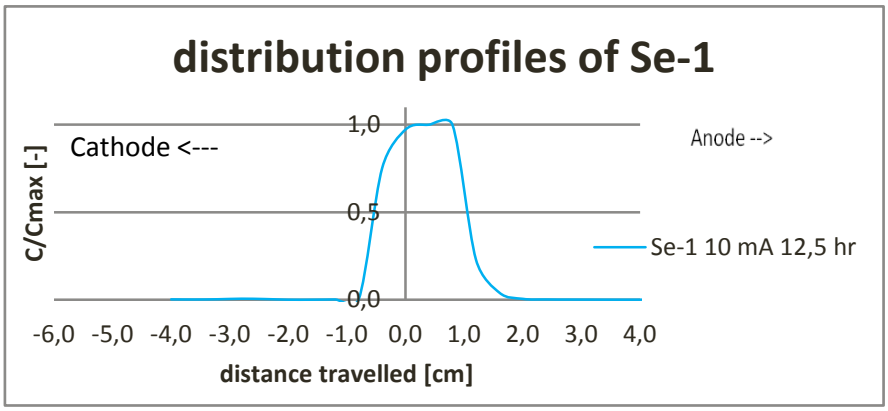


**Figure 19: Above) Distribution profiles of selenium under partially atmospheric conditions two species seem present. Below) Distribution profile of selenium two or three species seem present. The tracer was obtained by oxidizing seleniumdioxide with 1 M NaOH**

The first experiment was done with selenite at low current and hence a low electrical field. Much of the tracer remained in the origin. The area on the right side of the ordinate axis is larger than the area on the left side of the ordinate axis. This could mean that selenite is immobilized and mobilized again and further away immobilized again. There is also a small peak visible that is an artefact.

A second experiment was done under the same experimental condition expect for the electrical field and experimental time. A similar profile was obtained but the peak was located further from the origin. This second migration profile gives a stronger indication that we are dealing with two migration species (perhaps more). The migrating species could be selenite and selenate. However, no oxidizing compounds are known to be present. The Eh was not listed but it is highly unlikely that the SBCW had an oxidizing potential.

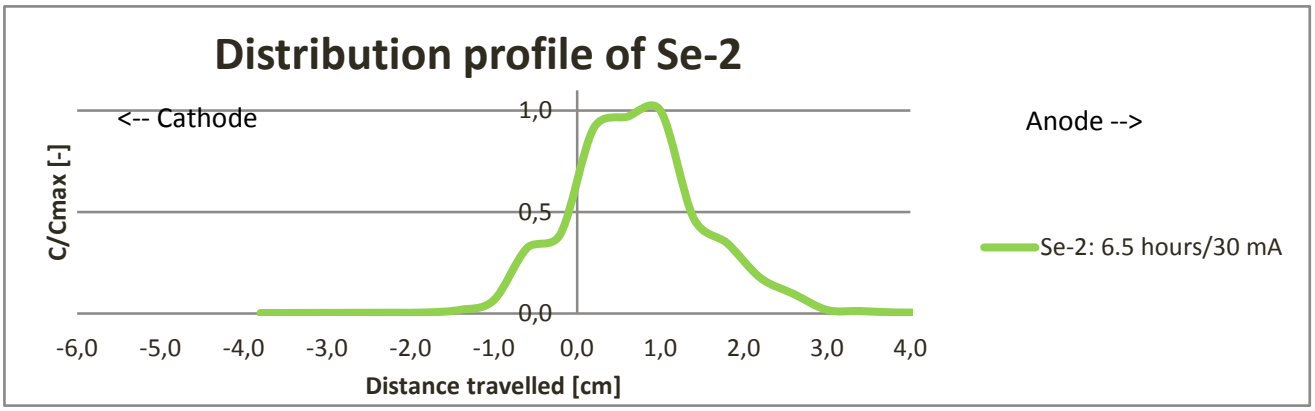


**Figure 20: Distribution profile obtained after the second experiment. The present of more than one species is more evident.**

The following experiments were conducted with selenate instead of selenite. Selenate experiments have been conducted before and were successful. To maintain an oxidizing environment, only $NaHCO_3$ was added to the SBCW. During the experiment the pH and Eh of the solution was adusted with two buffer solutions (pH 4, pH 7 and $NaHCO_3$)

The apparent molecular diffusion coefficient found for selenate is $1 \cdot 10^{-10}$ [$m^2/s$], which is according to literature ($5 \cdot 10 \cdot 10^{-10}$ [$m^2/s$]). With $K_d$-values taken from literature for selenium in Boom clay (0,2-1 ml/g) [8], a retardation factor between 1.3-2.6 was calculated. However, for more accurate results the $K_d$-value of selenium in bentonite should be determined.

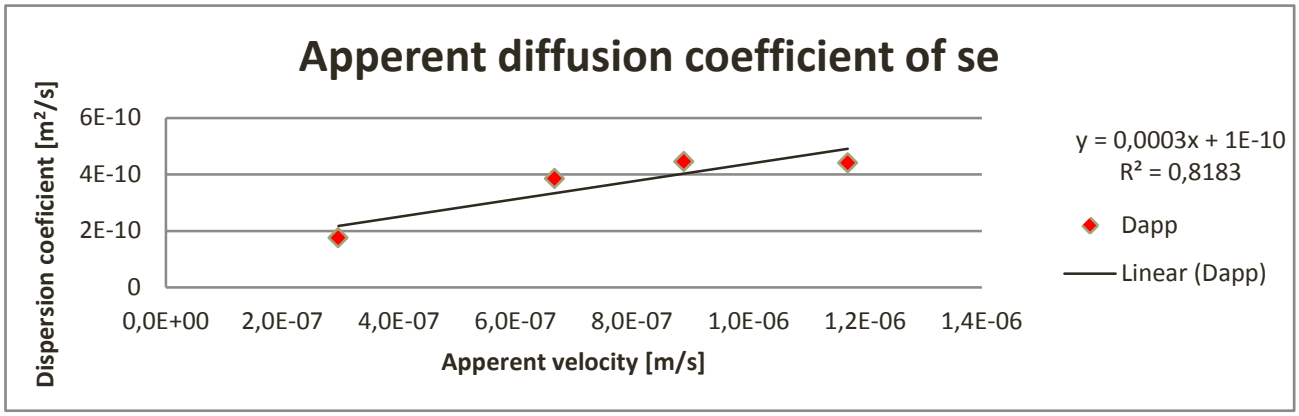


**Figure 21: Apparent diffusion coefficient obtained during the experiments with selenate.**

Unfortunately, the experiments with selenite did not work. It would have been more interesting to investigate the competition of pertechnetate with selenite than with selenate. Selenite forms strong inner-sphere complexes under the reducing conditions that are present in Boom clay. The retardation factor calculated raises suspicion that pertechnetate is retarded by the formation of the insoluble $TcO{\cdot}n(H_20)$. Both ions would compete over the hydroxyl of the $Al^{3+}$.

Although, selenate much less retarded it can also form outer-sphere complexes with the aluminium oxides, hence, we proceeded with the experiments. The experiments of selenium together with Technetium gave unexpected results (See Figure 22).

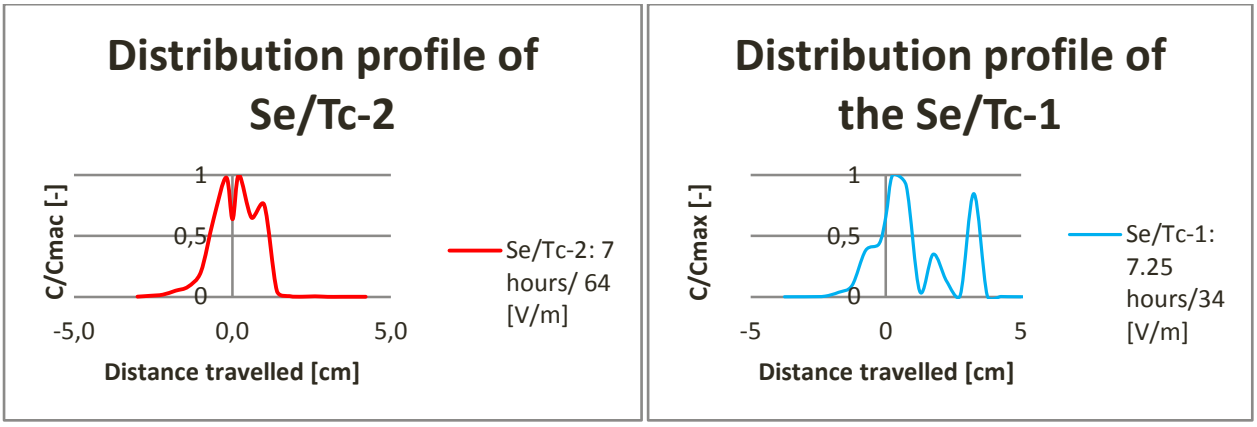


**Figure 22: Distributions profiles obtained for the combined Se/Tc experiments. Only radioactive technetium was used. The profiles indicate that technetium is immobilized and once again remobilized.**

In experiment Se/Tc-2, we see three peaks and in experiments Se/Tc-1, we see four peaks. Assuming the data is correct, the peaks in the distribution profiles could be explained by:

- Peak left of the origin. Strong electro-osmotic flow, which cannot be overcome by the migrating particles. However, this effect was not observed in the single experiment of Tc.
- Peaks right of the origin. Immobilization of the ions due to reactions with the $OH^-$ of the O-sheets. The different peaks were cause by remobilization of the Tc by $H_2O_2$. ( The selenate used in the experiment was dissolved in $H_2O_2$)

Tc seems to precipitate strongly here. However, a this pattern did not show in the single element tests. To determine whether the $H_2O_2$ caused the remobilization, a third experiment was conducted leaving out the selenium.

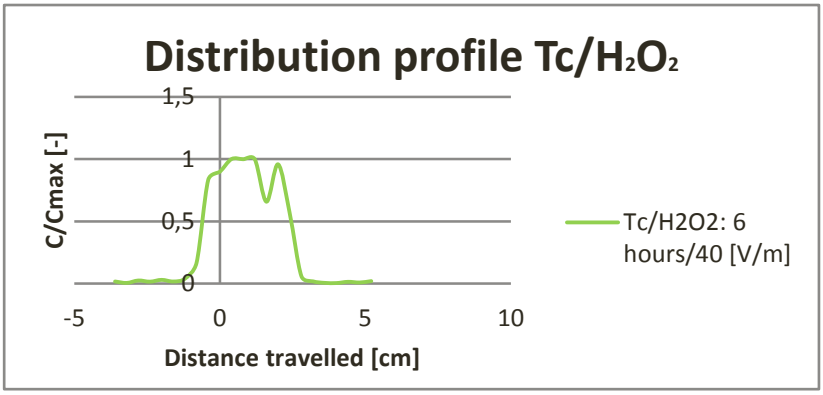


A similar pattern was obtained. It could be an indication that technetium is bond to form the hydrous ion, $TcO{\cdot}n(H_20)$ and then remobilized again. Hydrogen peroxide is capable of consuming the reductive capacity if the solid and thereby remobilizing Tc(+IV).

**Figure 23: Distribution profile obtained with Tc and hydrogen peroxide.**

Thus, the experiments with selenite were partially successful. Much of the selenite remained in the origin. This indicates that selenite is strongly sorbed. The distribution profiles of selenite had both more surface on the right side of the origin (toward the anode) this indicates that selenite is sorbed then desorbed to be sorbed again at a sorbing site located further away.

The experiments with selenate gave results that were in line with results found in literature The $D_{app}$ obtained was $1{\cdot}10{\cdot}10^{-10}$ [$m^2/s$] in literature a value of $5{\cdot}10{\cdot}10^{-10}$ [$m^2/s$] is found. To calculate the retardation $K_d$-values for selenate in Boom clay were taken. The retardation was calculated to be between 1.3 and 2.6. So, small retardation processes are present for selenate.

The combined experiments gave unexpected results. However, the distribution profile s believed to be caused by the hydrogen peroxide present in the experiment and not by the selenate. The distribution profile could be caused by the complexation of pertechnetate with the hydroxyl from the octahedral.

# 8. Conclusions

### *Electromigration cell*

The electromigration set-up suffered some problems. It was sensitive to flooding. This problem was solved by adding expansion barrels on top of the set-up. Also, the Fe(II) present in the SBCW showed to be a problem. The Fe(II)-atoms present became oxidized due to the oxygen being produced during electrolysis. When the Fe(II) oxidizes, it forms rust and quickly precipitates at the electrode. The rust changes the overall resistance of the migration cell and hence the electrical field over the sample. The oxidation was more serious at high current. The rust also damaged the electrode at the cathode. It is for this reason that the Fe(II) was left out in future experiments.

The external apparatus of the experimental set-up should be upgraded. The pumps would occasionally overheat. Replacing the monitoring devices (electrical field monitor, current monituor) would improve the results as constantly monitoring would be able then.

### *Ceasium*

Compared to results found by Kim et al. it can be concluded that the electromigration cell works properly. The apparent diffusion coefficients obtain ($4 \cdot 10^{-11}$ [$m^2/s$] and $7 \cdot 10^{-11}$ [$m^2/s$]) for respectively high and low current experiments) are in line with the apparent diffusion coefficients found by Kim et al. ($3.2 \cdot 10^{-11}$ [$m^2/s$]).

However, compared to Sato et al. the $D_{app}$ obtained is one order of a magnitude lower. This could be due to the way the clay sample was prepared. It was moulded by hand and the possibility exist that channels occurred.

The first set of experiments conducted with Cs also show that experimental time might be further reduced to six hours, when the electrical field applied is increased. However, so far mixing the results of the high current and low current experiment has not proven successful. The longitudinal dispersivity in the high current experiments was one order of a magnitude higher than in the low current experiments $3.7 \cdot 10^{-3}$ [m] vs. $3 \cdot 10^{-4}$ [m]). This is due to the higher velocity of the water through the sample, causing a larger dispersion.

### *Technetium*

The second set of experiments resulted in more convincing data on whether the electromigration cell works properly. The results obtained are more in line with literature than the results obtained for experiments with caesium. The apparent molecular diffusion coefficient obtained ($2 \cdot 10^{-10}$ [$m^2/s$]) is in good agreement with literature ($6.9 \cdot 10^{-10}$ [$m^2/s$]).

After only 3 hours, a typical and well-defined Gaussian distribution profile was obtained at a current of 40 mA. The experimental time for the different experiments was between 3 and 6 hours.

We also found a small retardation for pertechnetate. A small retardation factor was previously found to exist for pertechnetate in oxidizing conditions. The experimental condition here were slightly reducing, (Eh between -87 mV and -17 mV and pH ~8.5). The small retardation factor proves the retention of pertechnetate by either inner, - or outer-sphere complexes or by forming a sparingly insoluble hydrous oxide with the $OH^-$ of the O-sheets. As no iron was added to the SBCW, thus the possibility of Fe(II) oxidizing the pertechnetate can be excluded.

### *Selenium*

The experiments with selenite were partially unsuccessful. The first experiments yielded a graph that was more developed towards the anode. This could indicate that selenite is sorbed and desorbed and subsequently sorbed again to a second sorbing site. The second experiment was done at a higher current and shows a more deviating graph. Once again, the graph is developed more towards the right, but more peaks are visible. This could indicate more than one migrating species.

Possibly the selenite oxidized during the experiment. However, this is very unlikely due to the SBCW having a reductive potential. It could be due to the atmospheric environment. However, to exclude this possibility experiments under anaerobic conditions should be performed. A second possibility is the release of solubility-limit release of selenide.

The combined experiments with Tc and Se gave unexpected results. The migration profiles showed three peaks of technetium. As selenium dioxide was dissolved in hydrogen peroxide, this could indicate that the technetium was retarded by the formation of the insoluble $TcO{\cdot}n(H_20)$ with the hydroxyl ions from the clay and that it was then remobilized again, due to the hydrogen peroxide consuming the reductive capacity of the clay.

## Recommendations

In future experiments, it would be favourable to use the tubes or the experimental set-up to saturate the bentonite samples. In this way, the most homogenous samples can be obtained. Unsaturated samples may influence the experiments as that the degree of saturation determines the permeability of the clay sample.

The external equipment should be replaced by more adapted equipment. A new pump would increase the time experiments could run and a flow meter would enable to better adjust the flow from and toward the electrolyte compartments. Lastly, a current and electrical field monitor that is able to run a labview would enable to do experiments overnight and to intervene the experiments at an earlier stage. The set-up would sometime be pumped dry, when this happens the electrical field decreases. With labview, it would be possible to constantly monitor the set-up would and monitor changes in the electrical field.

Experiments conducted under fully anaerobic conditions should be performed to exclude the possibility of selenite oxidizing to selenate during the electromigration experiments, due to the oxidation of the clay.

More combined experiments of Tc and hydrogen peroxide should be conducted to determine whether the obtained results here can be reproduced.

The electromigration cell is especially suitable for strongly retained elements. Combined experiments on Ceasium and Sodium would be interesting. Both are retained by CEC and thus compete over the same binding place.

Selenate is relatively strong retained. It forms inner-sphere complexes. Experiments could be performed to determine it competes with other oxyanions. Silicate would be a good option, as it is also retained by the formation of inner-sphere complexes.

# References


1. No.419, G.S.o.J.O.F.R., *Atlas of Eh-pH diagramsIntercomparison of thermodynamic databases*, May 2005, National Institute of Advanced Industrial Science and Technology.
2. N. Maes, H.M., A. Dierckx, P. De Canniere, M. Put, *The assessment of electromigration as a new technique to study diffusion of radionuclides in clayeye soils.* Journal of Contaminant Hydrology, 1999. **36**(3-4): p. 231-247.
3. Breynaert, E., *Formation, Stability and Application of Eigencolloid Technetium and Chromium*, in *Departement Microbiele en Moleculaire Systemen*2008, K.U Leuven. p. 16.
4. Maes, N., *Ceasium rentention and migration behaviour in Boom Clay*, 2010, SCK-CEN. p. 1-89.
5. E. Verhoef, E.N., J. Grupa and A. Poley, *CORA Disposal concept clay*, 2011, COVRA. p. 2.
6. Euratom, *Geological disposal of radioactive waste produced by nuclear power ..from concept to implementation*, 2004.
7. Maes, N., et al., *The assessment of electromigration as a new technique to study diffusion of radionuclides in clayey soils.* Journal of Contaminant Hydrology, 1999. **36**(3–4): p. 231-247.
8. Pierre De Canniere, A.M., Steve Williams, Christophe Bruggeman, Thomas Bauwens, Norbert Maes and Mark Cowper, *Behaviour of Selenium in Boom Clay*, 2010, SCK*CEN: Mol. p. 54.
9. Christophe Bruggeman, S.S., Norbert Maes, *Americium retention and migration behaviour in Boom Clay*, 2012, SCK*CEN: Mol, Belgium.
10. Norbert Maes, S.S., Christophe Bruggeman, and E.M. Marc Aertsens, Van Laer Liesbeth, *Strontium retention and migration behaviour in Boom Clay*, 2012, SCK*CEN.
11. MITCHELL?, A.T.Y.a.J.K., *Coupled fluid, electrical and chemical flows in soil* Geotechnique, 1993. **43**(1): p. 121-134.
12. Viovy, J.-L., *Electrophoresis of DNA and other polyelectroytes: Physical mechanisms.* Modern Physics, 2000. **72**(3): p. 2.
13. Beauwens, T., et al., *Studying the migration behaviour of selenate in Boom Clay by electromigration.* Engineering Geology, 2005. **77**(3–4): p. 285-293.
14. Higashihara, T., et al., *Electromigration of sodium ions and electro-osmotic flow in water-saturated, compacted Na-montmorillonite.* Applied Clay Science, 2004. **26**(1-4): p. 91-98.
15. Higgo, J.J.W., *Clay as a barrier to radionuclide migration.* Progress in Nuclear Energy, 1987. **19**(2): p. 173-207.
16. Site, C.S.S. *Soil Texture - Physical Properties*. 2013 [cited 2013 20-9]; Available from: http://soilsurvey.cares.missouri.edu/tutorial/page8.asp.
17. GeoScienceWorld. [cited 2013 20-9]; Available from: http://elements.geoscienceworld.org/content/5/2/99/F2.large.jpg.
18. Ruedrich, J., et al., *Moisture expansion as a deterioration factor for sandstone used in buildings.* Environmental Earth Sciences, 2011. **63**(7-8): p. 1545-1564.
19. Korkiala-Tanttu, E.R.L., *Bentomap: Survey of bentonite and tunnel backfill knowlegde*, in *Mineralogical and chemical description of the bentonite material*2009, VTT Technical Research Centre of Finland: Finland. p. 3.
20. Jepson, A.P.F.a.W.B., *The exchange capacities of kaolinite and the preparation of homoionic clay.* Colloid and interface Science, 1975. **50**(2): p. 245-259.
21. Pansu, M. and J. Gautheyrou, *Anion Exchange Capacity.* Handbook of Soil Analysis: Mineralogical, Organic and Inorganic Methods, 2006: p. 755-766.
22. HAIM GVIRTZMAN 1, D.R.a.M.M., *ANION EXCLUSION DURING TRANSPORT THROUGH THE UNSATURATED ZONE.* Journal of Hydrology, 1983(87): p. 267-283.
23. Huysmans, M. and A. Dassargues, *Hydrogeological modeling of radionuclide transport in low permeability media: a comparison between Boom Clay and Ypresian Clay.* Environmental Geology, 2006. **50**(1): p. 122-131.

24. R.F. Mudde, M.T.K., V. van Steijn. *Molecules and Transport Phenomena*. 2013.
25. Van Loon, L.R., M.A. Glaus, and W. Müller, *Anion exclusion effects in compacted bentonites: Towards a better understanding of anion diffusion.* Applied Geochemistry, 2007. **22**(11): p. 2536-2552.
26. JRC. *Karlsruhe Nuclide Chart*. [cited 2013 01-08].
27. H. Sato, T.A., Y. Kohara, *Effect of dry density on diffusion of some radionuclides in compacted sodium bentonite.* Journal of Nuclear Science and technology, 1992. **29**(9): p. 873-882.
28. Tsai, S.-C., S. Ouyang, and C.-N. Hsu, *Sorption and diffusion behavior of Cs and Sr on Jih-Hsing bentonite.* Applied Radiation and Isotopes, 2001. **54**(2): p. 209-215.
29. Kim, H.-T., et al., *Diffusivities for ions through compacted Na-bentonite with varying dry bulk density.* Waste Management, 1993. **13**(4): p. 303-308.
30. Schwochau, K., *Technetium: chemistry and radiophamaceutical application*. 2000.
31. Firestone, L.P.E.a.R.B. 2004; Available from: http://ie.lbl.gov/toi/nuclide.asp?iZA=430099.
32. Zachara, J.I.W.M.N.Q.J., *The geochemistry of Technetium: A summary of the behavior of an artificial element in the natural enviroment*, in *PNNL-181392*008, Pacific northwest national laboratory: Washington. p. 3.1.
33. Serne, K.M.K.a.R.J., *Geochemical factors affecting the behavior of Antimony, Cobalt, Europium, Technetium and Uranium in Vadose sediments*, 2002, Pacific Northwest National Laboratory: United Stae of America. p. 5.6.
34. EPA, *Understandig the variation in partition coeffcient, Kd, values.* 2004. **III**: p. 13.
35. H. Vinsova, R.K., M. Koudelkova and V. Jedinakova-Krizova, *Sorption characteristics of $^{99}$Tc onto bentonite material with different additived under anaerobic conditions.* Radiochimica Acto, 2004. **94**(8): p. 435-44.
36. Sawatsky, N.G. and D.W. Oscarson, *Diffusion of Technetium in Dense Bentonite under Oxidizing and Reducing Conditions.* Soil Sci. Soc. Am. J., 1991. **55**(5): p. 1261-1267.
37. al., G.J.e., *Applied radiation and isotopes.* 2010: p. 68.
38. Wright, W.G., *Oxidation and mobilization of selenium by nitrate in irrigation drainage.* Enviromental Quality 1999. **IV**(28): p. 1182-1187.
39. Grambow, B., *Mobile fission and activation products in nuclear waste disposal.* Journal of Contaminant Hydrology, 2008. **102**(3–4): p. 180-186.
40. Bruggeman, C., et al., *Selenite reduction in Boom clay: Effect of FeS2, clay minerals and dissolved organic matter.* Environmental Pollution, 2005. **137**(2): p. 209-221.
41. Johnson, T.M. and T.D. Bullen, *Selenium isotope fractionation during reduction by Fe(II)-Fe(III) hydroxide-sulfate (green rust).* Geochimica et Cosmochimica Acta, 2003. **67**(3): p. 413-419.
42. Refait, P., L. Simon, and J.-M.R. Génin, *Reduction of SeO42- Anions and Anoxic Formation of Iron(II)−Iron(III) Hydroxy-Selenate Green Rust.* Environmental Science & Technology, 2000. **34**(5): p. 819-825.
43. Sato, H. and S. Miyamoto, *Diffusion behaviour of selenite and hydroselenide in compacted bentonite.* Applied Clay Science, 2004. **26**(1–4): p. 47-55.
44. T. Beauwens, P.D.C., H. Moors, L. Wang and N. Maes, *Studying the migration behaviour of selenate in Boom Clay by electromigration.* Engineering Geology, 2005: p. 8.
45. Robbin Martin, L.a.D.E.D., *Aqueous oxidation of sulfur dioxide by hydrogen peroxide at low pH.* Atmospheric Environment, 1981. **15**(9): p. 1615-1621.
46. S.M. Kunen, A.L.L., G.L. Kok and B.G. Heikes, *Aqueous oxidation of SO2 by hydrogen peroxide.* Journal of Geophysical Reseach, 1983. **88**(C6): p. 3671-3674.
47. Huffman, E.H., R.L. Oswalt, and L.A. Williams, *Anion-exchange separation of molybdenum and technetium and of Tungsten and rhenium.* Journal of Inorganic and Nuclear Chemistry, 1956. **3**(1): p. 49-53.
48. M. de Craen, L.W., M. van Geet and H. Moors, *Geochemistry of Boom Clay pore water at the Mol site*, 2004, SCK*CEN.

49. O. Karnland, S.O., U. Nilsson, *Mineralogy and sealing properties of various bentonites and smectite-rich clay materials*, in *TR-06-30*2006, Swedish Nuclear Fuel and Waste Management Co: Stockholm. p. 31-33.
50. García-Gutiérrez, M., et al., *Diffusion coefficients and accessible porosity for HTO and 36Cl in compacted FEBEX bentonite.* Applied Clay Science, 2004. **26**(1–4): p. 65-73.
51. Sigma-Aldrich. *Density 1 M NaOH*. 2013; Available from: http://www.sigmaaldrich.com/catalog/product/fluka/319511?lang=en&region=NL.

## A. Technical drawing electromigration cell

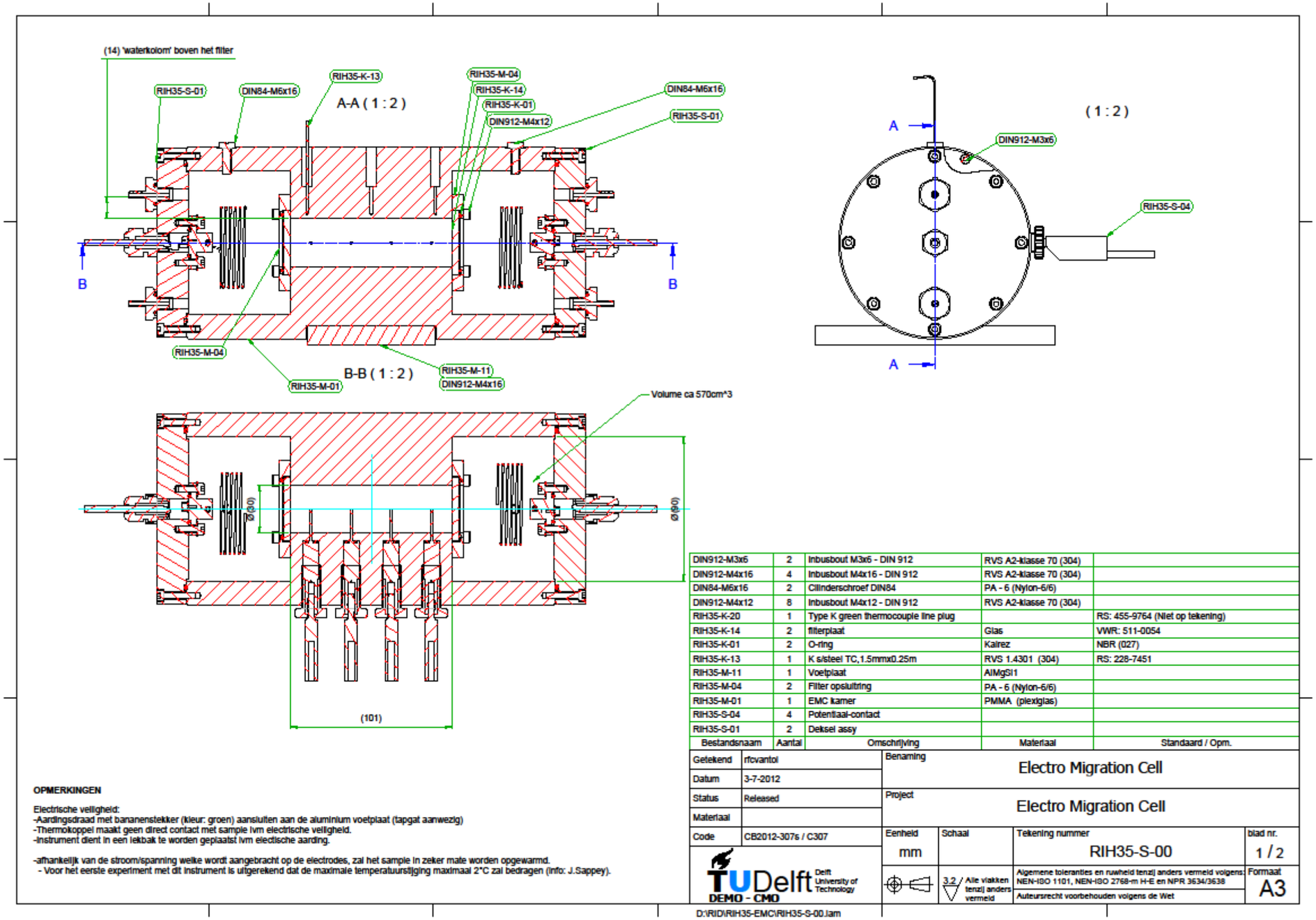


| | | | | |
|---|---|---|---|---|
| DIN912-M3x6 | 2 | Inbusbout M3x6 - DIN 912 | RVS A2-klasse 70 (304) | |
| DIN912-M4x16 | 4 | Inbusbout M4x16 - DIN 912 | RVS A2-klasse 70 (304) | |
| DIN84-M6x16 | 2 | Cilinderschroef DIN84 | PA - 6 (Nylon-6/6) | |
| DIN912-M4x12 | 8 | Inbusbout M4x12 - DIN 912 | RVS A2-klasse 70 (304) | |
| RIH35-K-20 | 1 | Type K green thermocouple line plug | | RS: 455-9764 (Niet op tekening) |
| RIH35-K-14 | 2 | filterplaat | Glas | VWR: 511-0054 |
| RIH35-K-01 | 2 | O-ring | Kalrez | NBR (027) |
| RIH35-K-13 | 1 | K s/steel TC,1.5mmx0.25m | RVS 1.4301 (304) | RS: 228-7451 |
| RIH35-M-11 | 1 | Voetplaat | AlMgSi1 | |
| RIH35-M-04 | 2 | Filter opsluitring | PA - 6 (Nylon-6/6) | |
| RIH35-M-01 | 1 | EMC kamer | PMMA (plexiglas) | |
| RIH35-S-04 | 4 | Potentiaal-contact | | |
| RIH35-S-01 | 2 | Deksel assy | | |
| Bestandsnaam | Aantal | Omschrijving | Materiaal | Standaard / Opm. |

**OPMERKINGEN**

Electrische veiligheid:
-Aardingsdraad met bananenstekker (kleur: groen) aansluiten aan de aluminium voetplaat (tapgat aanwezig)
-Thermokoppel maakt geen direct contact met sample ivm electrische veiligheid.
-Instrument dient in een lekbak te worden geplaatst ivm electische aarding.

-afhankelijk van de stroom/spanning welke wordt aangebracht op de electrodes, zal het sample in zeker mate worden opgewarmd.
- Voor het eerste experiment met dit instrument is uitgerekend dat de maximale temperatuurstijging maximaal 2°C zal bedragen (info: J.Sappey).

| | | | | | |
|---|---|---|---|---|---|
| Getekend | rfcvantol | Benaming | Electro Migration Cell | | |
| Datum | 3-7-2012 | | | | |
| Status | Released | Project | Electro Migration Cell | | |
| Materiaal | | | | | |
| Code | CB2012-307s / C307 | Eenheid: mm | Schaal | Tekening nummer: RIH35-S-00 | blad nr.: 1 / 2 |
| TU Delft Delft University of Technology DEMO - CMO | | 3.2 Alle vlakken tenzij anders vermeld | | Algemene toleranties en ruwheid tenzij anders vermeld volgens: NEN-ISO 1101, NEN-ISO 2768-m H-E en NPR 3634/3638 | Formaat: A3 |
| | | | | Auteursrecht voorbehouden volgens de Wet | |

D:\RID\RIH35-EMC\RIH35-S-00.iam

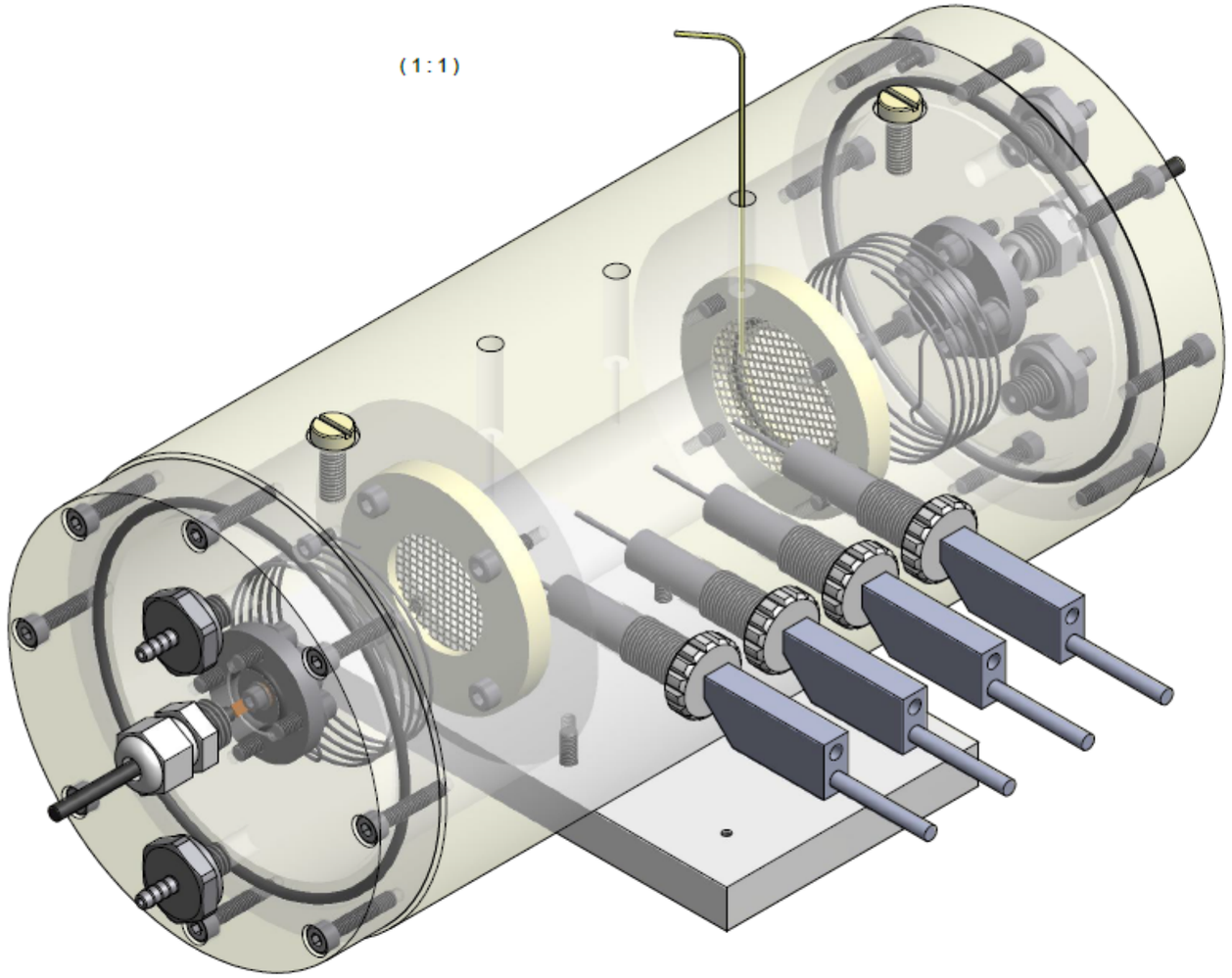


| | | | | | |
|---|---|---|---|---|---|
| Getekend | rfcvantol | Benaming | Electro Migration Cell | | |
| Datum | 3-7-2012 | | | | |
| Status | Released | Project | Electro Migration Cell | | |
| Materiaal | | | | | |
| Code | CB2012-307s / C307 | Eenheid: mm | Schaal: | Tekening nummer: RIH35-S-00 | blad nr.: 2 / 2 |
| TU Delft Delft University of Technology DEMO - CMO | | | 3.2 Alle vlakken tenzij anders vermeld | Algemene tolerantie en ruwheid tenzij anders vermeld volgens NEN-ISO 1101, NEN-ISO 2768-m H-E en NPR 3634/3638 | Formaat: A3 |
| | | | | Auteursrecht voorbehouden volgens de Wet | |

D:\RID\RIH35-EMC\RIH35-S-00.iam

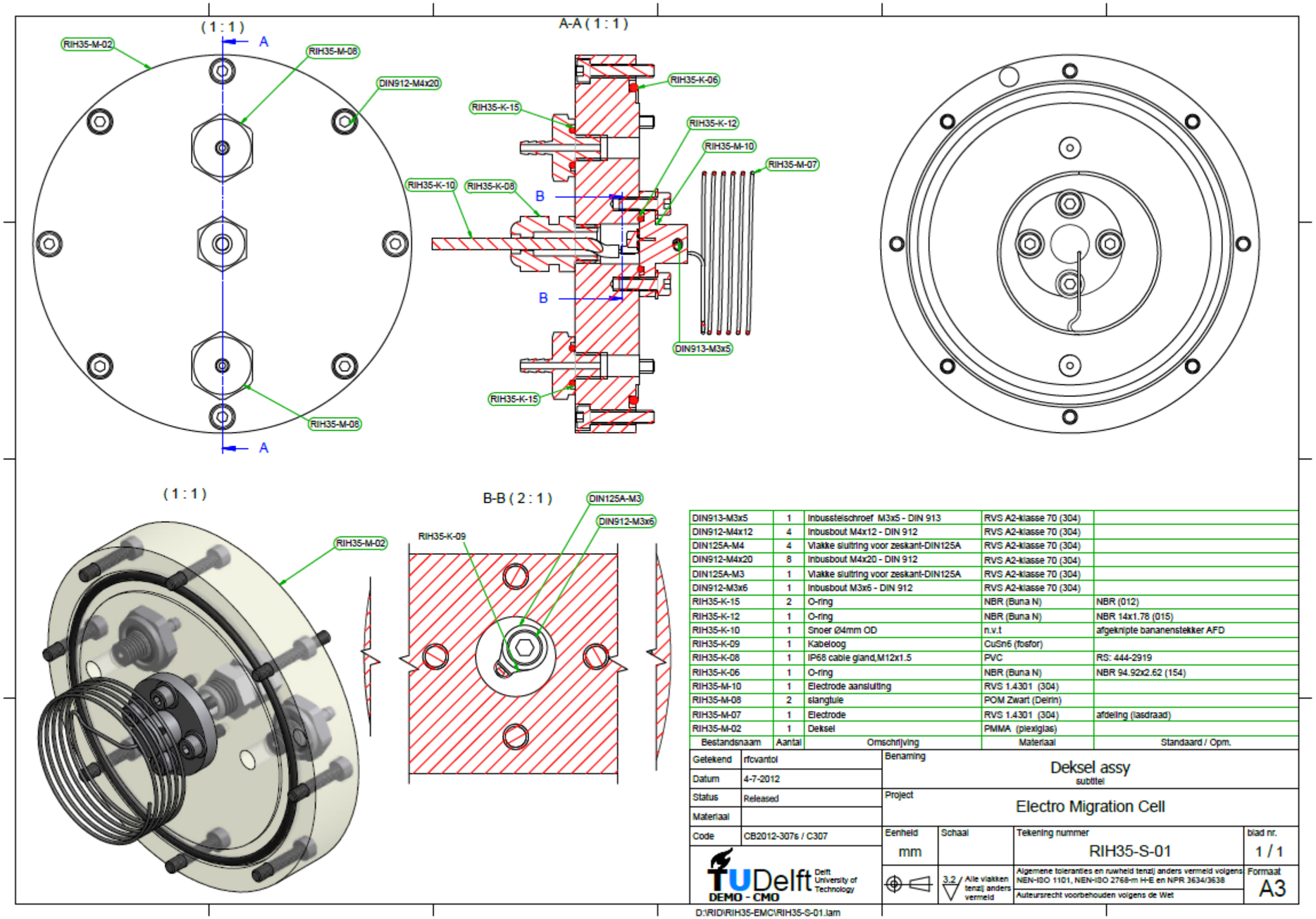


| Bestandsnaam | Aantal | Omschrijving | Materiaal | Standaard / Opm. |
|---|---|---|---|---|
| DIN913-M3x5 | 1 | Inbusstelschroef M3x5 - DIN 913 | RVS A2-klasse 70 (304) | |
| DIN912-M4x12 | 4 | Inbusbout M4x12 - DIN 912 | RVS A2-klasse 70 (304) | |
| DIN125A-M4 | 4 | Vlakke sluitring voor zeskant-DIN125A | RVS A2-klasse 70 (304) | |
| DIN912-M4x20 | 8 | Inbusbout M4x20 - DIN 912 | RVS A2-klasse 70 (304) | |
| DIN125A-M3 | 1 | Vlakke sluitring voor zeskant-DIN125A | RVS A2-klasse 70 (304) | |
| DIN912-M3x6 | 1 | Inbusbout M3x6 - DIN 912 | RVS A2-klasse 70 (304) | |
| RIH35-K-15 | 2 | O-ring | NBR (Buna N) | NBR (012) |
| RIH35-K-12 | 1 | O-ring | NBR (Buna N) | NBR 14x1.78 (015) |
| RIH35-K-10 | 1 | Snoer Ø4mm OD | n.v.t | afgeknipte bananenstekker AFD |
| RIH35-K-09 | 1 | Kabeloog | CuSn6 (fosfor) | |
| RIH35-K-08 | 1 | IP68 cable gland,M12x1.5 | PVC | RS: 444-2919 |
| RIH35-K-06 | 1 | O-ring | NBR (Buna N) | NBR 94.92x2.62 (154) |
| RIH35-M-10 | 1 | Electrode aansluiting | RVS 1.4301 (304) | |
| RIH35-M-08 | 2 | slangtule | POM Zwart (Delrin) | |
| RIH35-M-07 | 1 | Electrode | RVS 1.4301 (304) | afdeling (lasdraad) |
| RIH35-M-02 | 1 | Deksel | PMMA (plexiglas) | |

| | | | | | |
|---|---|---|---|---|---|
| Getekend | rfcvantol | Benaming | Deksel assy<br>subtitel | | |
| Datum | 4-7-2012 | | | | |
| Status | Released | Project | Electro Migration Cell | | |
| Materiaal | | | | | |
| Code | CB2012-307s / C307 | Eenheid: mm | Schaal | Tekening nummer: RIH35-S-01 | blad nr.: 1 / 1 |
| TU Delft Delft University of Technology DEMO - CMO | | 3.2 Alle vlakken tenzij anders vermeld | | Algemene tolerantie en ruwheid tenzij anders vermeld volgens NEN-ISO 1101, NEN-ISO 2768-m H-E en NPR 3634/3638<br>Auteursrecht voorbehouden volgens de Wet | Formaat: A3 |

D:\RID\RIH35-EMC\RIH35-S-01.iam

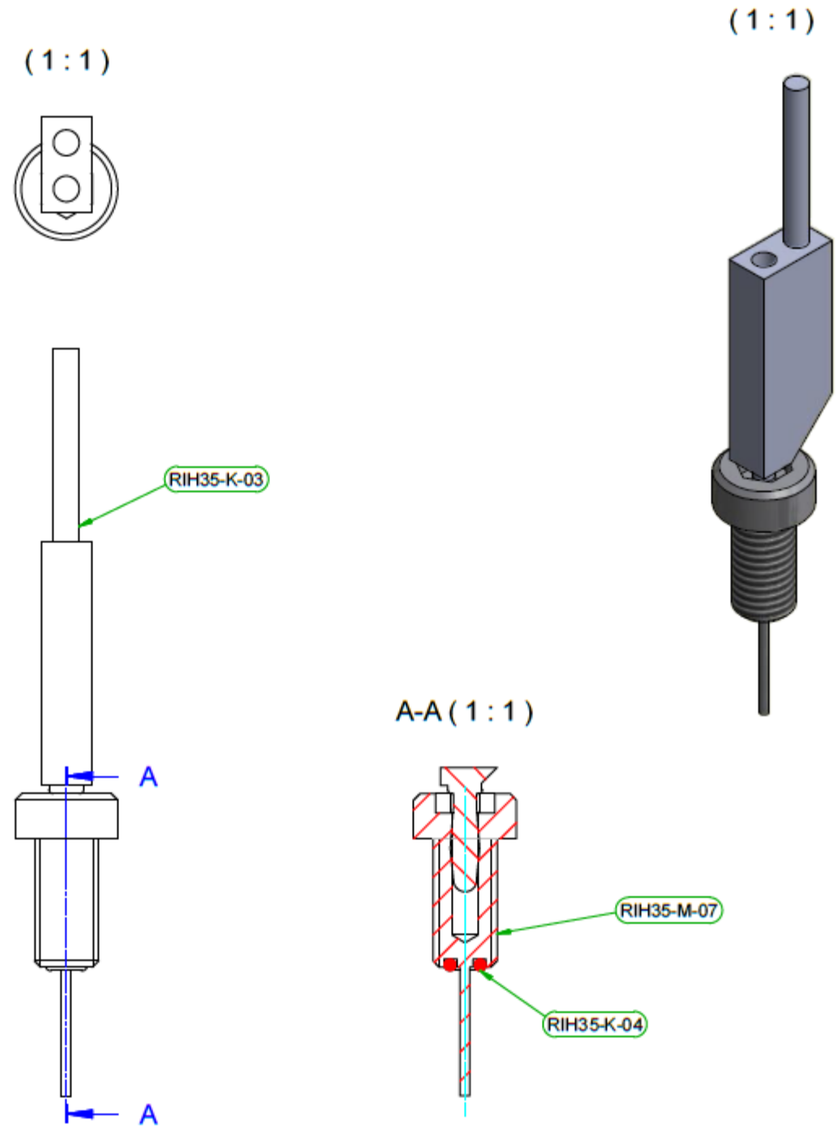


| | | | | |
|---|---|---|---|---|
| RIH35-K-04 | 1 | O-ring | NBR (Buna N) | NBR 2.9x1.78 (006) |
| RIH35-K-03 | 1 | Bananenstekker | n.v.t | afd |
| RIH35-M-07 | 1 | electrode | RVS A2-klasse 70 (304) | Inbusbout M10x40 - DIN 912 |
| Bestandsnaam | Aantal | Omschrijving | Materiaal | Standaard / Opm. |

| | | | | | |
|---|---|---|---|---|---|
| Getekend | rfcvantol | Benaming | Electrode assy<br>subtitel | | |
| Datum | 4-7-2012 | | | | |
| Status | WorkInProgress | Project | Project | | |
| Materiaal | | | | | |
| Code | CBxxx-xxxs / xxx | Eenheid | Schaal | Tekening nummer | blad nr. |
| TU Delft Delft University of Technology<br>DEMO - CMO | | mm | | RIH35-S-02 | 1 / 1 |
| | | Alle vlakken tenzij anders vermeld | | Algemene toleranties en ruwheid tenzij anders vermeld volgens NEN-ISO 1101, NEN-ISO 2768-m H-E en NPR 3634/3638<br>Auteursrecht voorbehouden volgens de Wet | Formaat A4 |

D:\RID\RIH35-EMC\RIH35-S-02.iam

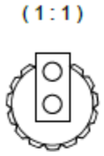

( 1 : 1 )

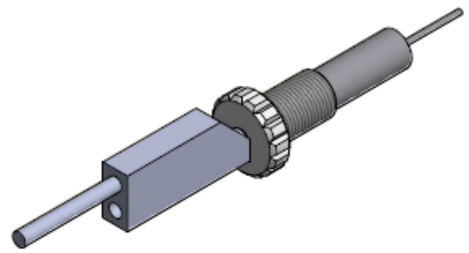

( 1 : 1 )

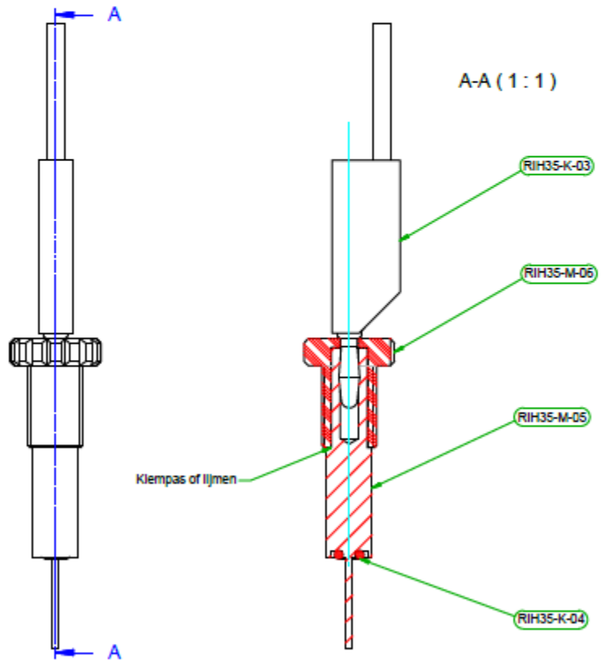


A-A ( 1 : 1 )

| | | | | |
|---|---|---|---|---|
| RIH35-M-06 | 1 | Isolatie draadstuk | POM (Delrin) | |
| RIH35-M-05 | 1 | electrode | RVS 1.4301 (304) | |
| RIH35-K-04 | 1 | O-ring | NBR (Buna N) | NBR 2.9x1.78 (006) |
| RIH35-K-03 | 1 | Bananenstekker | n.v.t | afdeling |
| Bestandsnaam | Aantal | Omschrijving | Materiaal | Standaard / Opm. |

| | | | | | |
|---|---|---|---|---|---|
| Getekend | rfcvantol | Benaming | Potentiaal-contact | | |
| Datum | 11-7-2012 | | | | |
| Status | Released | Project | Electro Migration Cell | | |
| Materiaal | | | | | |
| Code | CB2012-307s / C307 | Eenheid: mm | Schaal: | Tekening nummer: RIH35-S-04 | blad nr.: 1 / 1 |
| TU Delft Delft University of Technology DEMO - CMO | | | 3.2 Alle vlakken tenzij anders vermeld | Algemene toleranties en ruwheid tenzij anders vermeld volgens: NEN-ISO 1101, NEN-ISO 2768-m H-E en NPR 3634/3638 | Formaat: A3 |
| | | | | Auteursrecht voorbehouden volgens de Wet | |

D:\RID\RIH35-EMC\RIH35-S-04.lam

# B Synthetic Boom clay water

Deep unground the conditions are anaerobic, so if you plan on working in anaerobic conditions do not forget to degas your water. This could be done my bubbling nitrogen or argon through your flask over night. You can also leave your flask open in de glovebox to let he last ppm $0_2$ escape.

The recipe as given below is to produce 1 litre of SBCW. Add the following compounds to 1 litre of high quality water such as demi-water or bidistilled water. I used Mili-Q water.

Table 9: AMounts given in mg needed to prepare 1 litre of SBCW

| Salts | Quantity [mg] | MW | Mole/L |
|---|---|---|---|
| NaHCO3 | 1170 | 83,996 | 1,39e-2 |
| H3BO3 | 43 | 61,834 | 6,95e-4 |
| KCl | 25 | 74,555 | 3,35e-4 |
| MgCl2·6H2O | 22 | 203,218 | 1,08e-4 |
| NaF | 11 | 41,998 | 2,62e-4 |
| NaCl | 10 | 58,443 | 1,71e-4 |
| FeCl2 | 3 | 126,751 | 2,37e-5 |
| Na2SO4 | 0,3 | 142,041 | 2,11e-6 |
| Total dissolved salts | 1248,3 | | 1,55e-2 |

Further manipulations needed:

1. Supersaturation with 1000 mg of CaCO3 to adjust Ca2+. Stir for one week
2. Bubble the flask through with 0,4% CO2 and the remaining 99,6% can be either argon of nitrogen. Should be an inert chemical. Bubble through until the pH has stabilized.
3. Always filter through a 0,22 µm filter before use. In case of solybility experiments, perform an ultrafiltration through a 30000 MWCO filter
4. If you want to use the SBCW in combination with organic matter, add the organic matter after filtration

Table 10: Reference tabel to check the analyses of the SBCW

| Cations | Mol/L | MW | Mg/L |
|---|---|---|---|
| Na+ | 1,44$^{e}$-2 | 22,990 | 330,3 |
| K+ | 3,35$^{e}$-4 | 39,098 | 13,1 |
| Mg2+ | 1,08$^{e}$-4 | 24,305 | 2,6 |
| Ca2+ | | 40,078 | xx |
| Fe2+ | 2,37$^{e}$-5 | 55,845 | 1,3 |
| Total | 1,53$^{e}$-2 | | 347,3 |

| nions | Mole/L | MW | Mg/L |
|---|---|---|---|
| HCO3- | 1,39$^{e}$-2 | 61,017 | 849,9 |
| Cl- | 7,70$^{e}$-4 | 35,453 | 27,3 |
| F- | 2,62$^{e}$-4 | 18,998 | 5,0 |
| SO42- | 2,11$^{e}$-6 | 96,064 | 0,2 |
| Total | 1,50$^{e}$-2 | | 882,4 |

| Neutral species | Mole/L | MW | Mg/L |
|---|---|---|---|
| B(OH)3 | 6,95$^{e}$-4 | 61,834 | 43,0 |
| Total dissolved salts | | | 1272,8 |

# C Matlab script

```
clc;
clear all;
close all;

M=;               % s-1  (Insert intinal amount of activity)
S=;               % m2   (Insert surface of the clay slices)
t=;               % s    (Insert time in secondes)
x_aangebracht =0; % cm   (Insert location where tracer is spiked, if   done
                        correctly this should be the middle (0))

% Use the correct interpunction (dot/comma)
% Insert x in centimetres
% Below: Enter the location of the slices. Mind the matrix dimension.
x=[];
x=x./100;

% Normalize the activity by dividing A through Amax and enter below
c_norm=[];

% The next codes are to calculate the Vapp and Di
maxC=max(c_norm)
maxi=find(c_norm == maxC)
maxX=x(maxi)
Vapp=(maxX-x_aangebracht*0.01)/t;

options=optimset('Display','off');
Di0=1e-10;
x0=[Di0];

[fitx]=fminsearch(@formule,x0,options,x,c_norm,M,S,t,Vapp);
Di=fitx(1)
Vapp

c_calc=(M./(2.*S.*sqrt(pi.*Di.*t))).*exp(-((x- Vapp.*t).^2)./(4.*Di.*t));
c_calc=c_calc/max(c_calc);

 E=sum((c_calc-c_norm).^2)

 figure;
 plot(x,c_norm,'-*',x,c_calc,'-o');
 legend('measured','calculated');
 ylabel('c/c_0');
 xlabel('x [m]');

 end

 function E=formule(fitx,x,c_norm,M,S,t,Vapp)

 Di=fitx(1);

 c_calc=(M./(2.*S.*sqrt(pi.*Di.*t))).*exp(-((x-Vapp.*t).^2)./(4.*Di.*t));
 c_calc=c_calc/max(c_calc);

 % Compute the error in each concentration
 E=sum((c_calc-c_norm).^2);

 end
```

# D Determining the dry density

Before you can determine the dry density, you need to determine the grain density. The following steps have to be taken to obtain the grain density [49]:

(1) Dry 15 gram of clay samples at $105^0$C for 24 hour in a ventilated oven to remove adsorbed water.
(2) Take the samples out of the oven en quickly pour the samples into a volumetric flask and seal the flask and let it cool to room temperature. Do not forget to weigh the flask beforehand.
(3) Add 35 ml (or sufficient liquid) of 1 M or 3 M NaCl to the flask, until the sample is completely covered and seal the flask once again.
(4) Shake and rotate the sample for some time (an hour) to facilitate the air from escaping the bentonite
(5) Rest the sample for 24 hours
(6) Rotate the sample again and fill the sample with the rest of the test liquid until the flask in full.
(7) Weigh the flask with the test liquid and the clay sample

The grain density is determine using the following equation:

$$D_s = \frac{m_s}{V_{tot} - \frac{m_{tot} - m_{s+f}}{D_l}}$$

Where $m_s$ is the mass of the solid (clay sample after drying), $V_{tot}$ is the total volume, $m_{tot}$ is the total mass, $m_{s+f}$ is the mass of the solid and the flask and $D_l$ is the density of the liquid.

Once the dry density is determined you can calculate the dry density via the following equation:

$$D_d = \frac{D_s \cdot D_w}{D_s \cdot w + D_w}$$

Where $D_s$ is the grain density, as calculated above, $D_w$ is the density of water 1 kg/m$^3$ and w is the water ratio and can be calculated by:

$$w = \frac{m_w}{m_s}$$

Where $m_w$ is the mass loss due to drying the sample at $105^0$ C for 24 hours and $m_s$ is the remaining solid mass.

| Sample | Mass before drying | Mass after drying | Total mass $m_{tot}$ | Mass solid and fluid | Volume $V_{tot}$ | Density of test liquid [51] $D_l$ |
|---|---|---|---|---|---|---|
| **1** | 15,0 gram | 9,31 gram | 75,18 gram | 26,97 gram | 51,47 ml | 1.04 g/mL |
| **2** | 15,0 gram | 9,76 gram | 76,17 gram | 26,90 gram | 52,94 ml | 1.04 g/mL |